REVIEW

Check for updates

Recent progress in organic-based radiative cooling materials: fabrication methods and thermal management properties

Xin Li,[a] Zhenmin Ding,[a] Linghao Kong,[b] Xueying Fan,[a] Yao Li, [iD][c]
Jiupeng Zhao, [iD] *[a] Lei Pan,[a] Diederik S. Wiersma, [iD][def] Lorenzo Pattelli [iD] *[ef] and
Hongbo Xu [iD] *[a]

Organic-based materials capable of radiative cooling have attracted widespread interest in recent years due to their ease of engineering and good adaptability to different application scenarios. As a cooling material for walls, clothing, and electronic devices, these materials can reduce the energy consumption load of air conditioning, improve thermal comfort, and reduce carbon emissions. In this paper, an overview is given of the current fabrication strategies of organic-based radiative cooling materials, and of their properties. The methods and joint thermal management strategies including evaporative cooling, phase-change materials, fluorescence, and light-absorbing materials that have been demonstrated in conjunction with a radiative cooling function are also discussed. This review provides a comprehensive overview of organic-based radiative cooling, exemplifying the emerging application directions in this field and highlighting promising future research directions in the field.

1. Introduction

Global warming endangers the balance of natural ecosystems, affects human health and even threatens human survival.[1,2] Subsequently, reducing the "carbon footprint" of industrialized countries has become a global concern.[3] Already today, the decreased thermal comfort during the frequent and intense heat waves is inevitably leading to a reduction of work efficiency, irritability, and even health-related issues.[4-7]

Cooling is the most effective and straightforward strategy to maintain thermal comfort, and can be divided into active and passive cooling. Vapor-compression systems (such as refrigerators and air conditioners) represent the vast majority of active cooling appliances,[8,9] however they are characterized by significant electricity needs, exacerbate the heat island effect and global warming by

[a] *School of Chemistry and Chemical Engineering, Harbin Institute of Technology, Harbin, 150001, P. R. China. E-mail: jpzhao@hit.edu.cn, iamxhb@hit.edu.cn*

[b] *The first hospital of Jilin University, No. 1, Xinmin Street, Changchun City, Jilin Province, 130021, P. R. China*

[c] *Center for Composite Materials and Structure, Harbin Institute of Technology, Harbin, 150001, China*

[d] *Department of Physics and Astronomy, University of Florence, Sesto Fiorentino, 50019, Italy*

[e] *Istituto Nazionale di Ricerca Metrologica (INRiM), Turin, 10135, Italy. E-mail: l.pattelli@inrim.it*

[f] *European Laboratory for Non-linear Spectroscopy (LENS), Sesto Fiorentino, 50019, Italy*

dumping heat in the environment, and are associated with leakages of extremely potent greenhouse gases which are also harmful for our protective ozone layer. This is a major obstacle on our path to "carbon neutrality" and moreover it cannot provide cooling in open outdoor environments.[10] Although alternative active cooling methods such as water cooling,[11] air cooling,[12] and electrocaloric cooling[13,14] consume less energy, thanks to the large size and need for an electric-auxiliary system, they are unsuitable to wear. Entirely passive cooling, on the other hand, provides a much more flexible alternative for personal thermal comfort. Any object at non-zero temperature radiates heat in the form of electromagnetic waves.[15] The mid-infrared (MIR) wavelength range of 8–13 μm (atmospheric transparency window) coincides with the spectral peak of the thermal radiation from an object at ambient temperature, part of which can therefore escape from the Earth surface towards the cold sink of outer space.[16,17] This passive radiative cooling mechanism which requires no energy consumption and is conducive to sustainable development is therefore attracting increasing attention.[18-21] Before 2000, researchers only achieved radiative cooling during night-time hours or by shielding the radiator from direct sunlight, as a result of limitations in the fabrication techniques which could not deliver sufficient solar reflectivity and selective emissivity in the atmospheric transparency window.[22,23] With the improvement of micro–nano processing technology and self-assembly methods, daytime radiative cooling has now become a thriving research field offering an array of new functional materials for thermal management.

For achieving high cooling performance, the design and fabrication of spectrally selective materials with a high reflection of sunlight in 0.3–2.5 μm and strong emission in the atmospheric transparency window are of essential importance. Traditional radiative cooling materials are typically divided into functional layers that can realize reflection and emission. Our increasing ability to design and control the structural and spectral properties of these materials led to the development of new photonic structures at different micro and nano scales, including one-dimensional photonic crystals,[24] nanoscale multilayer film,[25] conical metamaterial pillar arrays,[26] and metamaterials of polar dielectric microspheres.[27] Such materials inevitably impose stringent requirements on nanofabrication such as vacuum evaporation,[19,28] ion etching[29] and electron beam lithography,[26,30] which can limit the practical applications of the materials due to their higher cost and long preparation times, and make it more difficult to apply the films on complex surfaces. On the other hand, easily applicable and commercially available white paint products cannot exert net daytime cooling, since one of their main components are TiO_2 nanoparticles which have a strong UV absorption.[31,32]

Organic-based materials are ubiquitous in our daily life thanks to their scalability, versatility, and easy manufacturing. Nowadays, more and more organic-based radiative cooling materials are processed to include air voids to promote ultra-broadband sunlight reflection and effective thermal-infrared emission,[33] such as nano-porous membranes,[34,35] nanofiber membranes,[36,37] organic–inorganic composite membranes,[38–40] and nano-porous gel with high reflectivity.[41,42] The main advantages of organic-based radiative cooling materials are their scalability, mechanical resistance and flexibility, weather resistance, and electric insulation, making them suitable for outdoor applications. Moreover, radiative cooling polymers coatings can be made free-standing, highly opaque and emissive at the same time, thus avoiding the need for an additional metal reflector substrate. Particularly, many polymers can be coated directly on any surface, which further simplifies the manufacturing and application process. The additional super-hydrophobicity and self-cleaning ability which is often exhibited by these coatings are also promising for their durability and the offered protection of the underlying materials. Importantly, even if these polymer coatings are eventually degraded by aging mechanisms, fall off, or get contaminated, they can be recycled and processed again using appropriate solvents to reduce waste material. Polymer-based radiative cooling textiles have also been proposed to meet the needs of "personal heat management", which is a simple and low-cost strategy to increase thermal comfort and reduce the need for active cooling.

It is well understood that the intrinsic absorption in the mid-infrared (MIR) region is typically associated with the intrinsic molecular bonding of the polymer.[43] At thermal equilibrium, the emissivity and absorptivity are restricted to be equal by Kirchhoff's law of thermal radiation.[44] This equivalence is used to guide the design of micro structured materials to further enhance their thermal emittance. Their distinctive structures make them appear white visually,[45] which is required for reflecting sunlight and minimizing the heat gain. In this paper, the currently available polymer-based radiative cooling materials are classified, and the typical methodologies, cooling capacities, and application scenarios are summarized. Table 1 summarize some crucial indicators of the polymer-based radiative cooler in recent years.

2. Theoretical calculation of daytime radiative cooling power

Radiative cooling power is an effective index to evaluate the comprehensive performance of materials, which is related to its practical applications. The atmospheric transmittance is higher in dry and sunny weather, which is more conducive in actual test of radiative cooling. In addition, wind speed, heat quality, humidity, solar irradiance, etc. also closely affect the cooling power of materials.[46]

As shown in schematic diagram (Fig. 1)[47] the net radiative cooling power (P_{net}) of the material mainly depends on the thermal outward radiative power by the cooler (P_{rad}), while the heat absorption comes from three parts (P_{abs}): absorbed incident solar radiation (P_{sol}), absorbed energy from atmospheric thermal radiation (P_{atm}), heat conduction–convection from ambient radiation ($P_{cond+conv}$).

When the radiative cooling device is placed under the sun, the P_{net} of the radiation material is given by the following equations:

$$P_{net}(T) = P_{rad}(T) - P_{atm}(T_{amb}) - P_{sol} - P_{(cond+conv)} \quad (1)$$

Thermal outward radiative power (P_{rad}):

$$P_{rad}(T) = \int^d \Omega \cos\theta \int_0^\infty d\lambda I_{BB}(T,\lambda)\varepsilon(\lambda,\theta) \quad (2)$$

Here, θ is the local zenith angle, $I_{BB}(T,\lambda)$ is the intensity of the radiation wave at the real-time temperature and the wavelength generated by the blackbody. $\varepsilon(\lambda,\theta)$ is the emissivity of the material at the wavelength λ.angular integral on the hemisphere:

$$I_{BB}(T,\lambda) = \frac{2hc^2}{\lambda^5} \frac{1}{e^{\frac{hc}{\lambda k_B T}} - 1} \quad (3)$$

Here, T is spectral radiation temperature of Blackbody, h is the Planck's constant. k_B is the Boltzmann constant, c is the speed of light, λ is wavelength.

Absorbed incident solar radiation (P_{sol}):

$$P_{sol} = \int_0^\infty d\lambda \in (\lambda, \theta_{sol}) I_{AM1.5}(\lambda) \quad (4)$$

where, $I_{AM1.5}(\lambda)$ is the AM 1.5 spectral distribution of solar radiation. θ_{sol} is the inclination of the radiation refrigeration device facing the sun.

Absorbed energy from atmospheric thermal radiation (P_{atm}):

$$P_{atm}(T_{amb}) = \int d\Omega \cos\theta \int_0^\infty d\lambda I_{BB}(T_{atm},\lambda)\varepsilon(\lambda,\theta)\varepsilon_{atm}(\lambda,\theta) \quad (5)$$

$$\varepsilon_{atm}(\lambda,\theta) = 1 - t(\lambda)^{\frac{1}{\cos\theta}} \quad (6)$$

Table 1 Summary of information on various types of polymer radiative cooling materials

Structure	Material	Preparation method	Reflectivity	Emissivity	$\Delta T_{\text{amb-cooler}}$	Cooling power	Remarks	Ref.
Nanofiber-based membrane	PEO	Roll-to-roll electrospinning	96.3%	78%	5 °C	110 W m^{-2}	Selective thermal emitter	52
Nanomesh fibers textile	PVDF	Electrospinning	$\approx 90\%$	—	12 °C	—	50% IR transmittance for human body	56
Porous textile	Porous PVDF films	Melt spinning and *in situ* microfibrillar method	94.2%(Vis)	94.5%	17.7 °C	—	—	57
Porous coatings	P(VdF-HFP)	Phase inversion-based method	$96 \pm 0.03\%$	$97 \pm 0.02\%$	6 °C	96 W m^{-2}	Can be coated on any substrate surface and self-supporting	34
Porous membrane	(P(VdF-HFP))	Phase separation	92%	96%	6.3 °C	—	Can work as a thermo-electric generator	60
Porous membrane	[P(VdF-HFP)HP]	Spray-phase-separation	97.2%	93.5%	14.9 °C	62 W m^{-2}	Large coverage of cars	61
Built-in 3D micropores membrane	PDMS	Facile sacrificial template method	93.4%	94.6%	5.8 °C	112 W m^{-2}	3D microvoid arrays embedded in a PDMS	65
Nano-micro-structured plastic	Amphiphilic methacrylic acid	Locally confined polymerization based on tunable liquid–liquid phase separation	$\approx 96\%$	$\approx 90\%$	8.6 °C on electronic circuits	140 W m^{-2}	Can used for electronics' thermal management	68
Porous membrane with cross-linking structure	PVDF and PUA	Photo-initiated free-radical polymerization	93.36%	93.33%	8.28 °C	94.2 W m^{-2}	—	70
Hollow micro-fiber membrane	PVDF and PVA	Coaxial electrospinning	94%	94%	9 °C	—	Low thermal conductivity	73
Porous membrane with hydrogel	Li-PAAm hydrogel and P(VdF-HFP)	Photopolymerization and phase inversion method	96%	96%	7 °C	150 W m^{-2}	Evaporative cooling combine with radiative cooling	79
Tri-layer composite textile	PA/PVDF/PE	Electrospinning	>90%	—	refrigerated the human body by 6.5 °C	72.78 W m^{-2}	Reduce thermal conductivity	82
Nanoprocessed silk	Al$_2$O$_3$ nanoparticles and nature silk	Coupling reagent-assisted dip-coating method	95%	$\approx 90\%$	3.5 °C	—	Enhance the reflectivity in the UV wavelength region	51
Photonic film	h-BN and PDMS	Hot-pressing method	98%	90.3%	4 °C	—	Low thermal resistance simultaneously	95
Nanofiber film	K$_2$Ti$_6$O$_{13}$ nanofiber and PEO	Electrospinning	95.4%	94.8%	≈ 8 °C	92 W m^{-2}	Absorb high-energy UV photons, improving the mechanical stability and UV durability	98
Fiber membrane	PU and Si$_3$N$_4$ nanoparticles	Electrospinning	91%	93%	21.9 °C	—	Janus wettability and heat conduction	106
Hierarchical metafabric	CA/Al$_2$O$_3$ nanoparticles and PA6/SiO$_2$ nanoparticles	Electrospinning and dipcoating processes	99.16% (0.3–0.76 μm) 88.60% (0.76–2.5) μm	78.13%	16.6 °C	—	Wick-evaporation cooling (~ 8.2 °C)	107
Hierarchical-metafabric	TiO$_2$-PLA laminated with a thin PTFE layer	Melt extrusion mixing, melt spinning and drafting	92.4%	94.5%	≈ 4.8 °C	—	Commercial sewing techniques	110

where, T_{amb} is the ambient temperature, ε_{atm} (λ, θ) is the atmospheric emissivity at zenith angle θ and wavelength λ.

Heat conduction–convection from ambient radiation ($P_{\text{cond+conv}}$).

$$P_{\text{cond+conv}}(T, T_{\text{amb}}) = h_{\text{cc}}(T_{\text{amb}} - T) \qquad (7)$$

where, h_{cc} is the non radiative heat transfer coefficient, in low humidity climate, the typical non radiative heat transfer coefficient h_{cc} is 0–12 W m^{-2} K^{-1} [48,49] The heat transfer performance is greatly affected by the location of radiation, humidity and other factors,

and the actual temperature of materials is greatly affected by a variety of factors.

3. Development of single-polymer radiative cooling materials

Single-polymer radiative cooling materials are typically made of fiber membranes and porous membranes. Additionally, some studies have also reported on polymeric gels achieving net cooling performance. In these materials, the fiber diameter and/or pore
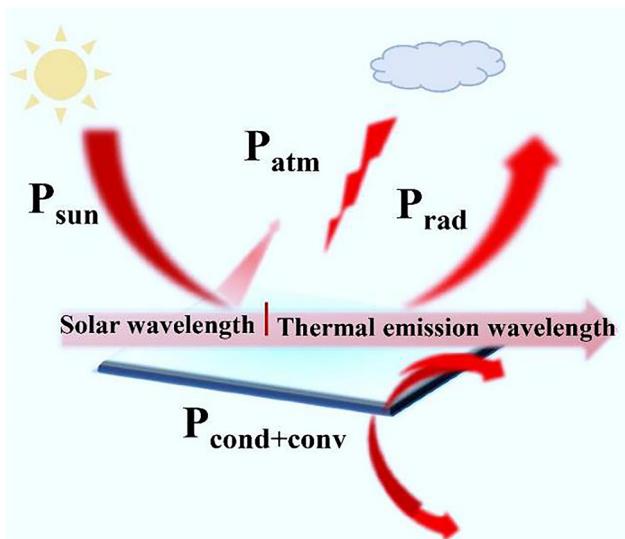
Fig. 1 The thermal energy flow in a typical daytime radiative cooling system. Reproduced with permission from ref. 47. Copyright 2022, Wiley-VCH GmbH.

size distributions in the membranes can be optimized based on Mie theory to achieve high reflection over the broad solar spectrum.[50–52] At present, radiative cooling fabrics offer high design versatility, since the spatial weaving of the fabric, the fiber size and texture, as well as the micro–nano structure inside the fiber provide a hierarchy of structures that can be engineered to target different spectral regions, thus optimizing the efficiency of the spectral response while avoiding interference between different regions.

3.1 Fiber materials of single-polymer

Electrospinning,[53] melt spinning,[54] and wet spinning[55] can be used to prepare ultra-thin flexible fiber membrane with controllable

porosity, greatly increasing the specific surface area of the membrane compared to conventional fabrics. This allows to tune near-infrared and infrared optical properties simply by tailoring the properties of the textile structure rather than introducing specialized components or other composite materials in the fabrication process. The infrared emissivity of the polymer can be controlled by the choice of its functional groups. A scalable PEO nanofiber-based membrane (Fig. 2a) with fiber diameters distributed in the 500–1200 nm range was demonstrated by Li et al.[52] using roll-to-roll electrospinning (Fig. 2b). A reflectivity of 96.3% was achieved in the 0.3–2.5 μm wavelength range, while selective emissivity (78% in 8–13 μm) was endowed by the C–O–C ($1260-1110$ cm^{-1}) and C–OH ($1239-1030$ cm^{-1}) bonds, leading to a sub-ambient temperature drop of $|\Delta T| \approx 5$ °C even under the peak solar intensity of near 900 W m^{-2}. A nanomesh textile using commercial polyvinylidene fluoride (PVDF) fibers with ~ 600 nm average diameter exhibited over 90% solar reflectance, and a 12 °C temperature drop, better than that observed with fiber diameters of 203 nm and 490 nm.[56] The light scattering ability of larger fibers can be enhanced by increasing their porous scattering surface, which is relevant for fibers obtained via melt-spinning that would be too large to provide a sufficient reflectivity at visible wavelengths. Song et al.[57] prepared a spectrally selective PVDF graded porous textile for radiative cooling clothing through the process of melt-spinning and PEO removal (Fig. 2c), where the incompatibility between PEO and PVDF was used to tune the fiber porosity (Fig. 2d), resulting in a porous PVDF textile with high mid-infrared emittance (94.5%), and opacity of solar irradiation at near-infrared (90.3%) (Fig. 2e). Under direct solar irradiation, the porous PVDF textile reduced overheating with respect to the bare case by more than 17 °C at peak, suggesting a significant improvement for personal thermal comfort.
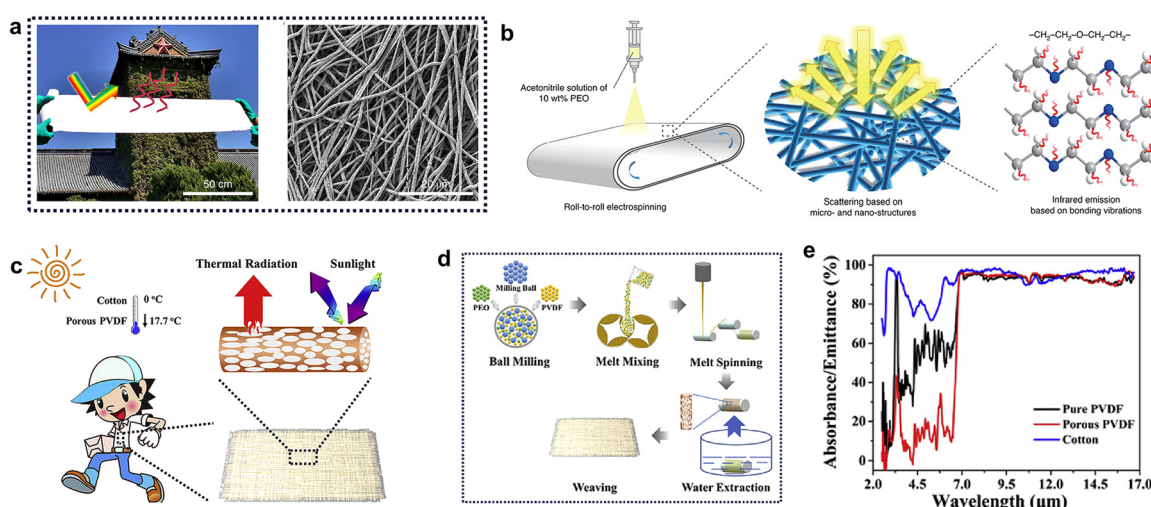
Fig. 2 (a) The photo (left) and SEM image of disordered nanofibers (right) the of the electrospinned PEO nanofibre-based membrane. (b) Schematic illustration of roll-to-roll electrospinning fabrication process (left) for micro-and nano-structured film (middle) schematic diagram of PEO molecular chain bond vibration (right). Reproduced with permission from ref. 52. Copyright, 2021 Nature Publishing Group. Schematic illustration of (c) porous PVDF textile, and (d) manufacturing process of the PVDF fibre. (e) The near-infrared and mid-infrared absorbance/emittance curves of porous PVDF, pure PVDF and cotton. Reproduced with permission from ref. 57. Copyright, 2020 Elsevier.

3.2 Porous materials of single-polymer

Porous polymer membranes can reach a high scattering efficiency, thanks to the refractive index contrast at the air/solid interfaces of their micro and nano-structured morphology. In addition to the preparation of porous fiber films by spinning, phase separation methods are highly suitable for the preparation of polymer porous membranes, which are simpler and easier for fabricating large-area porous membranes and have been shown to reach record-high scattering efficiencies.[58,59] Polyvinylidene fluoride-hexafluoropropylene (P(VdF-HFP)) has attracted much attention due to its relatively low UV absorption, high intrinsic emission, and good stability. Mandal *et al.*[34] firstly prepared a P(VdF-HFP) membrane with multi-scale micro–nano porous structures depending on the different evaporation rates of acetone and water (Fig. 3a and b). The solar reflectance (96%) and long-wave infrared emittances (97%) of the hierarchically porous membrane allow for sub-ambient temperature drops of ∼6 °C under solar intensities of 890 W m^{-2}. Compared with fibrous membranes, this material can be coated on any surface

or become a self-supporting membrane (Fig. 3c). Inspired by the work above, another P(VdF-HFP) porous membrane with a porosity larger than 60% was prepared in deionized water by a phase separation method, achieving a solar reflectance of 92% and an atmospheric window emissivity of 96%.[60] Further improvements on this preparation strategy have been proposed, mainly to improve the control over the structure formation and its porosity distribution. Since the volatilization of solvent is accompanied by the movement of the molecular chain, the thickness of the film is poorly controlled, which will affect the stability of its reflectivity. Shorter film formation times would therefore be desirable to minimize this effect. A promising spray-phase-separation strategy was applied by Wang *et al.*,[61] in which the slurry is atomized into small droplets during the spraying process, and phase separation occurs thereon (Fig. 3d). The large amount of air introduced during the spray process allows to control the mesoporous structure of thick membranes and achieve rapid prototyping, guaranteeing uniform pore sizes over large areas (Fig. 3e–g). The fabricated P(VdF-HFP) flexible
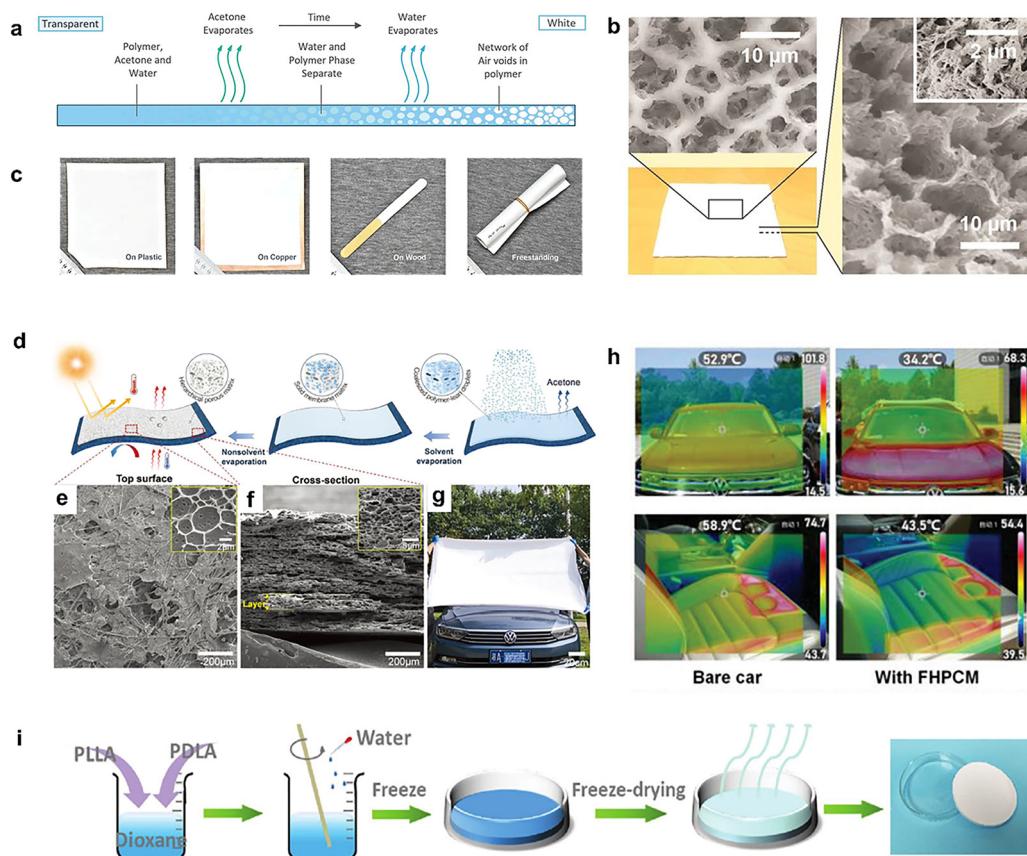
Fig. 3 (a) Schematic illustration of the phase transformation process of forming a hierarchically porous P(VdF-HFP) membrane from a solution of acetone (solvent), water (non-solvent) and P (VdF-HFP). (b) The SEM images of the top and cross-section of P(VdF-HFP) membrane. Inset: The SEM of its nanoporous. (c) Hierarchically porous P(VdF-HFP) can be coated on plastics, copper, and wood, and made into a strong, flexible, and freestanding sheet. Reproduced with permission from ref. 34. Copyright 2018, American Association for the Advancement of Science. (d) Schematic illustration of spray-phase-separation method and passive daytime radiative cooling principle of FHPCM used as car shed under sunlight. The SEM images of FHPCM (e) top surface, (f) cross-section, (g) optical photo of large FHPCM. (h) IR photographs and temperature measurements of two real cars: one is covered with FHPCM, and the other is without a cover. Top image: real-time temperature of the front and internal air of the two cars. Bottom image: temperature difference (ΔT) of the front and internal air between the two cars. Reproduced with permission from ref. 61. Copyright 2021, Wiley-VCH GmbH. (i) Fabrication process of the superhydrophobic PLA aerogel. Reproduced with permission from ref. 63. Copyright 2022, Wiley-VCH GmbH.

hierarchically porous complex membrane (FHPCM) with 73.5% porosity realized an average reflectance of 97.2% 0.24–2.5 μm, and an emittance of 93.5% in the atmospheric window. In addition to building walls and wearable materials, this FHPCM can be used to cool down the interior space of a vehicle even in adverse heat and humidity conditions, reaching a maximum temperature difference of 18.7 °C (Fig. 3h). The thermally induced phase separation technology can accelerate the volatilization of solvent and realize the interconnection pore network structure in the film. Park et al.[62] prepared biodegradable polylactic acid (PLA) film by this method, making it an environment-friendly radiative cooler. Coincidentally, Liu et al.[63] successfully constructed superhydrophobic PLA aerogel with biomimetic hierarchical structure and high stereocomposite crystal content based on water-assisted thermally induced phase separation method (Fig. 3i). Its solar reflectivity can reach 89%, and the infrared thermal emissivity can reach 93%.

In addition to the phase separation-based method, the sacrificial template method can be adapted to prepare porous polymer membranes with controlled pore size. Due to the densely arranged microporous array structure designed on the surface and the randomly distributed nanoscale pores, the membranes can efficiently scatter sunlight and increase the thermal emissivity.[64] Among them, SiO$_2$ microspheres, polystyrene (PS) microspheres, salt, and sugar are often used as templates. In this case, polydimethylsiloxane (PDMS) is often used for its selective emissivity. Zhou et al.[65] used PS microsphere arrays as templates and prepared a PDMS membrane with built-in 3D micropores (Fig. 4 a–d).

The membrane exhibited a 93.4% solar reflectance and 94.6% emissivity into the atmospheric window, showing a ~5.8 °C temperature drop under the membrane. Notably, if the template used for pore forming is environmentally friendly and recyclable, the manufacturing process is more sustainable, with no volatile or residual toxic solvent.[66] Zhou et al.[67] proposed a sugar sacrificial template to realize a porous PDMS sponge that can effectively suppress heat exchange for a combination of radiative cooling and thermal insulation properties (Fig. 4d). The cooling capacity of the resulting sponge is higher than that of commercial white paint, with a temperature drop of ~4.6 °C under direct sunlight during the day. Sponges and gels are common liquid-absorbing and heat-insulating materials. The radiative cooling capability can be further enhanced based on the porous structure of the gel polymer, and the synergy between its low thermal conductivity and evaporative cooling properties. Regarding the cooling of electronic devices, a nano–micro-structured plastic with reconstruction and regeneration ability developed by Gao et al.[68] exploiting locally confined polymerization (LCP) of a Amphiphilic methacrylic acid (MAA) solution (Fig. 4e) achieved 90% thermal emissivity and 96% reflection between 500 and 1500 nm. When placed on top of an electronics, the temperature is 8.6 °C lower than what would be obtained by commercial polycarbonate (Fig. 4f). More importantly, environmentally sustainable plastic can also decrease resource waste and plastic pollution. Materials with good thermal insulation can reduce heat conduction between the internal and external environment and optimize cooling capacity at high temperatures, which has interesting applications also for the cooling of water,
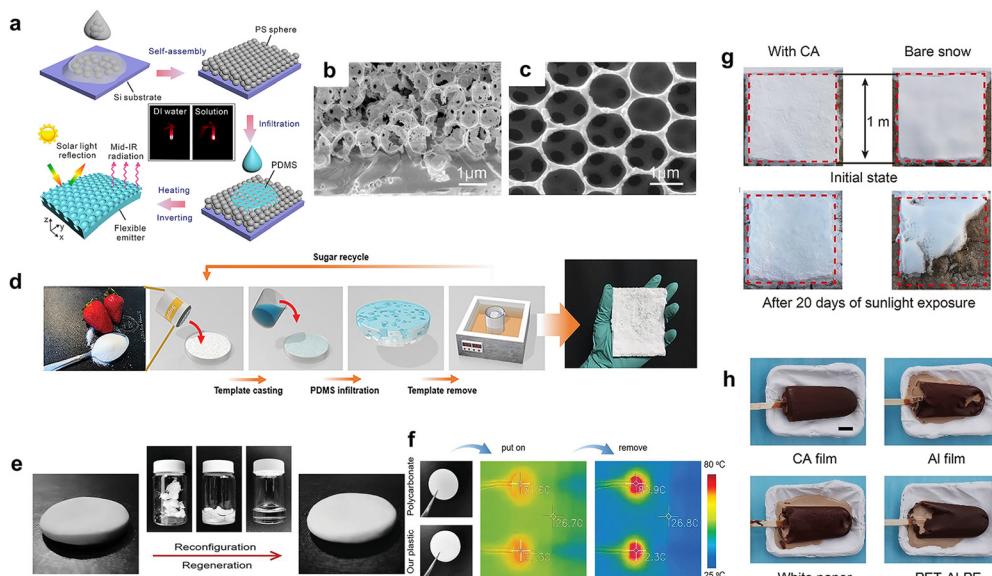
Fig. 4 (a) Schematic illustration of the fabrication process of the 3D microporous PDMS membrane. SEM images of the (b) embedded 3D micro pore array and (c) surface image of the 3D micro-void membrane. Reproduced with permission from ref. 65. Copyright 2021, American Chemical Society. (d) Schematic illustration of the manufacturing process for porous PDMS sponges. Reproduced with permission from ref. 67. Copyright 2021, Wiley-VCH GmbH. (e) The photographs of the polycarbonate wafer and the nano-micro-structured plastic with the same dimensions. (f) The infrared thermal images of the electronic circuits covered by different materials, and after the removal of the covering materials. Reproduced with permission from ref. 68. Copyright 2021, Wiley-VCH GmbH. (g) Optical photos of the ice creams placed in different material (CA film, Al film, white paper, and PET-Al-PE) after ~80 min under the sunlight (~540 W m^{-2}). Scale bar: 2 cm. (h) Optical photos of the initial state and after 20 days of the snow under the CA film and without the cover in outdoor sunlight. Reproduced with permission from ref. 69. Copyright 2022, American Association for the Advancement of Science.

food, or portable devices. Li *et al.*[69] have recently shown a hierarchically designed cellulose acetate (CA) radiative cooling films which is capable of slowing down significantly the melting of ice even under direct sunlight. In a test with an ice cream, about 98% of it was still preserved by the CA film after 80 min, as compared to white paper, Al, and PET-Al-PE bags (Fig. 4g). After 20 days of outdoor sunlight exposure, the melting rate of snow can also be significantly reduced with the protection of the CA film (Fig. 4h), which might therefore even serve to protect glaciers from global warming.

4. Development of composite-polymer radiative cooling materials

Combining two or more polymers into a composite radiative cooling material allows to add multiple functionalities and exploit the advantages of each component. Different polymers

can be blended in solution to prepare microscopically unified composite films, or different polymers can be combined in layers each of which can provide different spectral properties or the coupling of different cooling mechanisms.

4.1 Synergistic compounding of various polymers

The reflection mechanism of composite polymer membranes manufactured by phase separation and spinning is the same as that of single polymer membranes, but they can fully combine the inherent vibration absorption of different polymers in the infrared region which is beneficial to broadening and improving the emissivity of the composites.

A porous membrane of PVDF/polyurethane-acrylic (PUA) with a stable cross-linking structure was obtained *via* photo-initiated free-radical polymerization (Fig. 5a and b).[70] Its anti-glare surface finish reduced the light pollution when used as a material to mitigate the urban heat island effect. The synergy of the two materials increased the durability and stability under
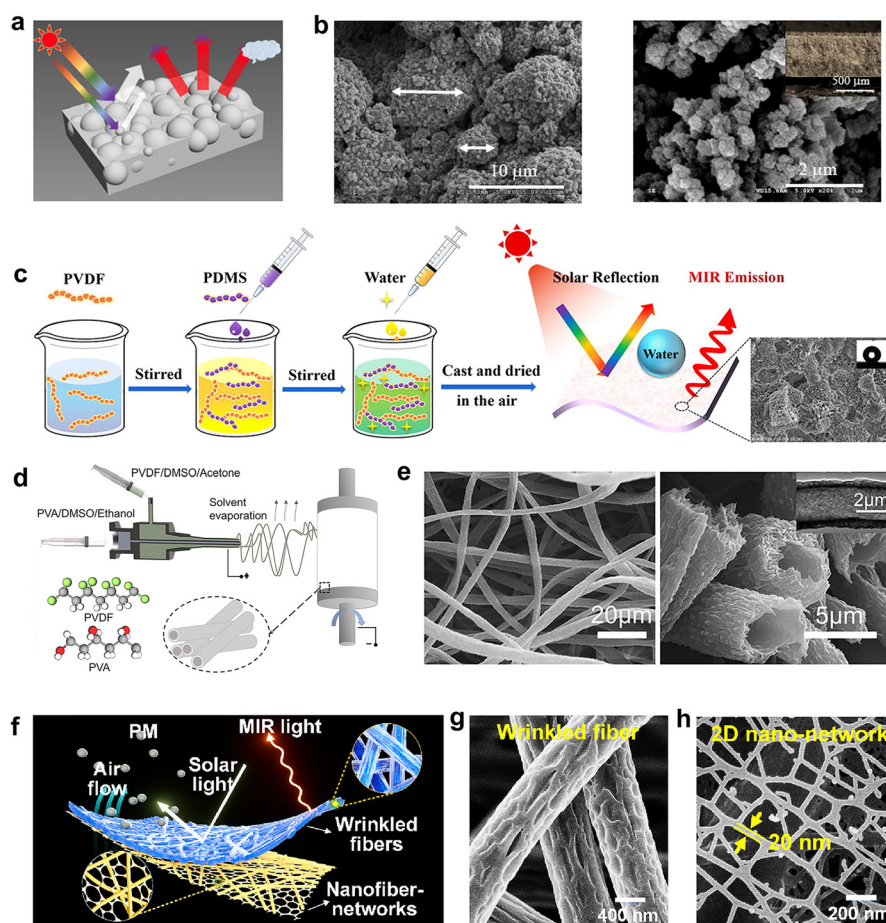
Fig. 5 (a) Schematic illustration of the PVDF/PUA porous membrane and its passive daytime radiative cooling principle. (b) Top-view and cross-sectional SEM images of the PVDF/PUA membrane. Reproduced with permission from ref. 70. Copyright 2020, American Chemical Society. (c) Schematic illustration of the phase-separation technique for superhydrophobic PDMS/PVDF porous membrane, and free-standing radiative cooling membrane. Reproduced with permission from ref. 72. Copyright 2022, Elsevier. (d) Schematic illustration of the coaxial electrospinning process for hollow microfibers, (e) The SEM images of the hierarchically hollow microfibers at various magnifications. Reproduced with permission from ref. 73. Copyright 2021, American Chemical Society. (f) Schematic illustration of the radiative cooling nanofiber networks with filtration capacity. (g) The SEM image of produce wrinkled P (VDF–HFP) nanofibers, (h) 2D PVDF nanostructure network. Reproduced with permission from ref. 74. Copyright 2022, American Chemical Society.

outdoor conditions. The strong UV radiation resistance, corrosion resistance, hydrophobicity, and good self-cleaning ability of outdoor refrigeration materials are also important factors affecting their long-term use and widespread application. In recent research, polymer based materials have been extensively studied. Zou et al.[71] developed a nonsolvent-induced phase separation (NIPS) method combined with ambient pressure drying to prepare polyethylene–polysilicate all-polymer porous coatings without using inorganic particles that are difficult to disperse uniformly. It has a Cyphochilus beetle-like skeleton structure, realizing a win–win situation for optical and mechanical properties. A PDMS/PVDF porous membrane was also similarly obtained through a phase separation process by Huang et al.[72] (Fig. 5c), which achieved excellent cooling performance with a high solar reflectance of 97%, a mid-infrared (MIR) emissivity of 96%, and a remarkable sub-ambient cooling of 12.3 °C under direct sunlight. A frequent feature of composite fiber membranes is to have hierarchically hollow microfibers with low thermal conductivity. Following this principle, Zhong et al.[73] prepared a hollow microfiber membrane by coaxial electrospinning of PVDF and PVA (Fig. 5d and e), reaching 94% solar reflection and 94% infrared emission, yielding a temperature drop of about 9 °C under a sunlight irradiance of 900 W m^2. Compared to electrospinning fiber, a multi-functional fiber material which also offers thermal insulation due to its internal microstructure, holds promise also for future eco-friendly building applications. Liu et al.[74] developed a new preparation method of polymer fiber membrane, and prepared an air conditioning mask with high performance particulate matter (PM) pollution removal and thermal/humidity/breathing comfortability through electrospinning/netting technology (Fig. 5f). The humidity induced double solidification and phase separation of the electrospinning jet were manipulated to produce wrinkled P (VDF-HFP) nanofibers as a radiative cooling layer (Fig. 5g), and the unique electronetting technique sprayed charged droplets generated by Taylor cone into liquid film under external force, and then separates the phases to form a two-dimensional polyvinylidene fluoride (2D PVDF) nanostructure network (composed of interconnected nanowires), which is used as the core filtration layer (Fig. 5h). The heterogeneous radiative cooling nanofiber networks structure of the mask leaded to efficient removal rate of PM$_{0.3}$ (>99.988%) and significant radiative cooling capacity (about 2.8 °C temperature drop).

4.2 Collaborative composition of multi-function layer

In the case of multilayer composite polymer radiative cooling membranes, generally, the upper and lower membranes play the role of solar high reflection and infrared high emission, respectively.[45] Low-cost and available porous PE films are often used as reflective layers due to their high scattering efficiency and transparency in the wavelength range of the atmospheric window,[75] as it only comprises aliphatic C–C and C–H bond. When combined with a strongly emitting substrate (such as PDMS[76] or human skin[77]) porous PE membrane or PE textiles can still transmit out thermal radiation while providing sufficient breathability and wearing comfort. Polymers are suitable for preparing large radiative cooling films. Tian et al.,[78] used
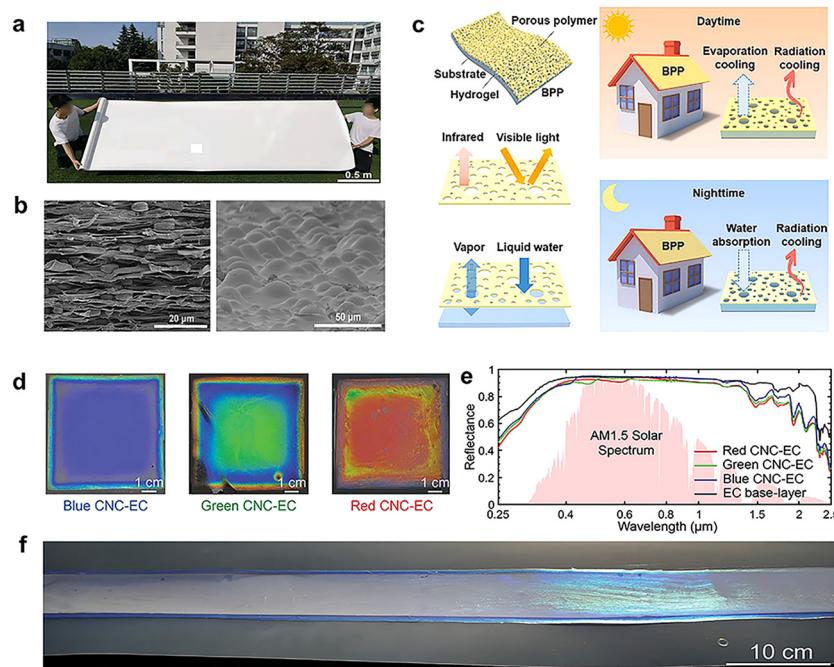
Fig. 6 (a) Photograph of the super-large-scale hierarchically porous film. (b) The SEM image of cross-sectional porous film with hierarchical eye-like air pores inside (left) and the PMMA micro-hemisphere coated on the porous film (right). Reproduced with permission from ref. 78. Copyright 2022, Wiley-VCH GmbH. (c) Optical performance and vapor evaporation of the bilayer porous polymer for intelligent building cooling. Reproduced with permission from ref. 79. Copyright 2021, Elsevier (d) macroscopic images and (e) spectral UV-Vis-IR reflectivity of EC film and blue, green, and red CNC−EC bilayer films. (f) large area film under natural light. Reproduced with permission from ref. 83. Copyright 2022, Wiley-VCH GmbH.

film-stretching method and based on the incompatibility between PET and polyolefin, prepared a super-large-scale hierarchically porous film (HPF)with polyolefin short pillars at the center of the air pores to separate the top and bottom PET layers (Fig. 6a). As MIR lenses for focusing and consequently to improve the emissivity. A layer polymethyl methacrylate (PMMA) micro-hemisphere was coated on the HPF to improve the emissivity to 90.1% (Fig. 6b). In addition, they can also reduce the specular light pollution of HPF, which is conducive to outdoor applications. Radiative cooling membranes can also be combined with layers providing other types of passive refrigeration methods (evaporation cooling) to further improve their cooling capacity. For instance, a bilayer porous polymer (BPP) radiative cooling device composed of a PAAm hydrogel soaked in aqueous LiBr solution (Li-PAAm hydrogel) (bottom layer) and a porous P(VdF-HFP) membrane (top layer) has been recently proposed (Fig. 6c).[79] In the daytime, the double-layer membrane shows the synergistic effect of evaporation and radiation cooling, while in the night when the temperature decreases, the film can prevent overcooling. This is because when the ambient temperature decreases, the high affinity between Li^+ and surrounding water vapor is conducive to a regeneration of the Li-PAAm hydrogel which releases heat to neutralize the radiative cooling effect. Due to this effect, the double-layer membrane can achieve a sub-ambient temperature decrease of 7 °C under direct sunlight. Traditional textiles are also used as substrates of composite membranes to enhance their mechanical strength and reduce thermal conductivity.[80,81] The cooling performance of a nylon (PA)/PVDF/polyethylene (PE) tri-layer composite textile,[82] for instance, was approximately 2.5 times higher than that of traditional natural textiles in terms of perceived outdoor personal thermal comfort, thanks to the combined scattering effect of the three layers, reaching a high reflection (90.22%) in the visible range and leading to a skin temperature decrease by 6.5 °C. The naturally derived cellulose nanocrystals (CNC) are extracted from renewable resources such as cotton and wood pulp. They can be self-assembled into colloidal liquid crystals with cholesteric order in water. After water evaporation, this left-handed cholesteric ordered film can selectively reflect visible light according to the periodic changes of the CNC helicoidal structure to produce adjustable structural colors (Fig. 6d). This kind of CNC film coated on highly scattering porous ethyl cellulose (EC) substrate can simultaneously achieve broadband solar reflection (>90% in 0.4–2 μm) (Fig. 6e). It also shows efficient radiative cooling (Day: −4 °C, Night: −11 °C).[83] Most importantly, the preparation technology of this color radiative cooling film has realized the large-scale production of roll to roll (Fig. 6f).

5. Development of organic–inorganic composite radiative cooling materials

The weather resistance, acid and alkali resistance, flame retardant, and stability of organic–inorganic composite membranes are typically superior to that of organic membranes. For example, the refractive index of most organic materials in the visible range is limited at around 1.5,[84] which is lower than most metal oxides such as $BaSO_4$ (1.63)[85] Al_2O_3 (1.77),[86] ZnO (2),[87,88] and TiO_2 (2.7).[89] Furthermore, the unique Si–O, Si–O–Si bonds of SiO_2 and its phonon-polariton resonance can make it used as the filler of high IR emissivity polymer.[47] By combining these materials and tuning the size distribution of inorganic fillers, the spectral reflectance and emissivity of radiative cooling materials can thus be further regulated. In this section, we will focus on the research progress of organic–inorganic composite radiative cooling membranes.

5.1 White inorganic filler composite polymer

The most obvious effect of adding inorganic fillers into the polymer matrix is to enhance the light scattering ability.[90,91] In addition, they can also promote the formation of voids and pores in the phase separation process. While the emissivity of the membranes depends on the intrinsic emissive nature of the polymer and inorganic fillers.[92] The undesired absorption of the polymer to UV light (accounting for 4.6–6.2% of total solar radiation) will weaken the overall solar reflectance and reduce the cooling effect. Especially in tropical areas, stronger UV irradiation may prohibit cooling.[93] Inorganic nanoparticles with high refractive indexes can be used to reduce the absorption of UV, thereby increasing solar reflectance. For instance, Al_2O_3 nanoparticles have high reflectivity in the UV, and the refractive index difference with respect to the natural silk helps preserving the wearability of silk and achieving a stronger solar reflection(Fig. 7a).[51] Inorganic fillers with even higher bandgaps can help reduce solar absorption in the UV range. $BaSO_4$ has a large band gap (6.0 eV), which shows high reflectivity from UV to NIR wavelength. The synergistic effect of the ideal internal characteristics of randomly dispersed $BaSO_4$ nanoparticles and the strong Mie scattering of porous ethyl cellulose phase separation coating (Fig. 7b) made the ultrawhite coating (Fig. 7c) have 98.6% solar reflectivity and 98.1% thermal emission.[94] In addition, the low UV absorption and fire resistance of 2D hexagonal boron nitride (h-BN, bandgap = 5.96 eV) can be a desirable feature for applications in the building sector. Li et al.[95] reported a method for introducing h-BN dielectric nanoplates into PDMS to prepare a scalable photonic film. The unique 2D shape and the high backscattering efficiency of h-BN endowed the photonic films with high solar reflectivity and low thermal resistance at the same time, 98% solar reflection and 90.3% emissivity in the 8–13 μm range can be achieved. Moreover, compared to pores, using dielectric nanoplates as fillers can break the trade-off between light reflection and heat dissipation of traditional radiation, especially for above-ambient radiative cooling applications (Fig. 7d). The large band gap of h-BN corresponds to the absorption of light with a wavelength less than 250 nm, meaning it is conducive to the low low solar heat gain.[96] Chan et al.[97] used 2D boron nitride nanosheets (BNNS) exfoliated from bulk h-BN powders and additive freeze-casting technique with waterborne polyurethane (WPU) as matrix to prepare decimeter-scale aerogel panel with consistent planar inner pore arrangement (Fig. 7e–g). The high inplane k of BNNS can make the heat flow arrange along the pore arrangement
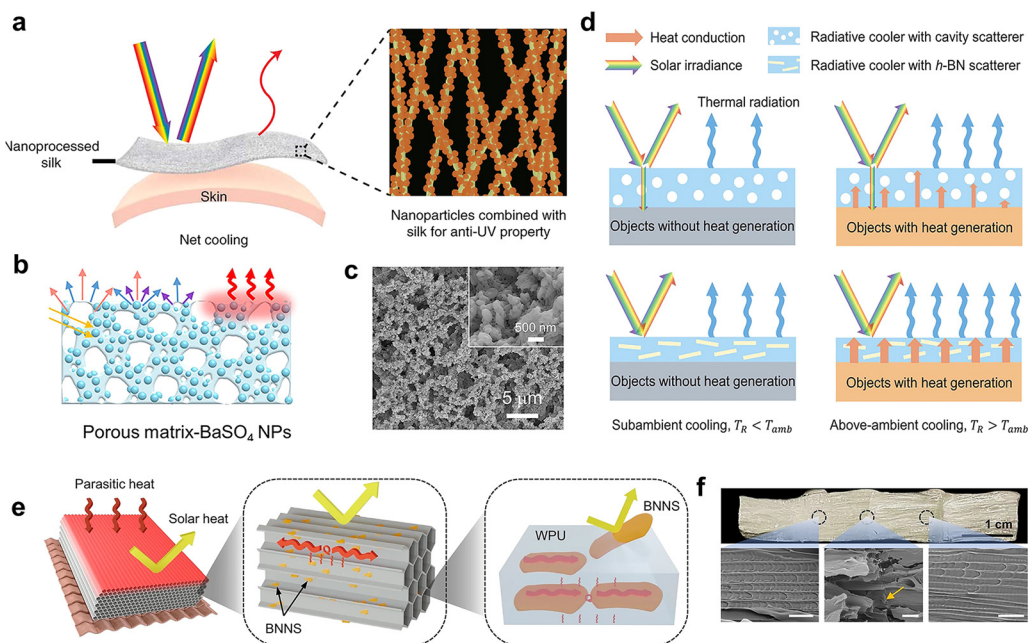
Fig. 7 (a) Schematic illustration of Al_2O_3 nanoprocessed silk by enhancing UV reflectance. Reproduced with permission from ref. 51. Copyright 2021, Nature Publishing Group. (b) Schematic illustrations of optical performance and (c) the SEM images of porous ethyl cellulose and $BaSO_4$ NPs phase separation coating. Reproduced with permission from ref. 94. Copyright 2022, American Chemical Society. (d) Schematic illustration composition and structure of decimeter-scale aerogel panel. Reproduced with permission from ref. 95. Copyright 2022, Wiley-VCH GmbH. (e) Schematic illustration of decimeter-scale aerogel panel. (f) Photograph and SEM images of the showing the decimeter-scale aerogel panel with uniform pore arrangement. Reproduced with permission from ref. 97. Copyright 2022, Nature Publishing Group.

direction, thereby inhibiting the heat transfer in the thickness and reducing the heat gain, so that this structure shows ultra-low out of plane thermal conductivity (16.9 m W m^{-1} K^{-1}). The solar reflectivity of the composite material is up to 97%. Recent research by Yao et al.[98] showed that the $K_2Ti_6O_{13}$ (PT) nanofibers are high-energy UV photon absorption material, which were added to PEO fiber matrix to generate a small amount of current and heat by absorbing UV light to resist UV aging failure (PT@ PEO) (Fig. 8a and b) without affecting the cooling performance, and the mechanical stability of the polymer matrix was improved substantially (Fig. 8c). The doping of chopped glass fibers in P(VdF-HFP) aerogels is expected to improve its mechanical strength and integrity. In addition, the glass fibers created additional scattering interfaces in the matrix, which further helped to improve the total reflection of sunlight. Glass fiber can also improve the compression resistance and flame retardancy of the composite.[99]

Inorganic fillers can also be used to enhance the emission of composites in the mid-infrared (MIR) region. Among them, the intrinsic infrared absorbance of Si–O bond (8.5, 9.4, and 12.5 μm), Si–O–Si bond (9.1 μm), and Si–N bond (11 μm) are widely used to enhance emissivity.[100,101] Additionally, SiO_2 has a strong absorptivity peak near 9 μm due to its phonon-polariton resonance.[27] The combination of SiO_2 microspheres (6–14 μm diameter) and nanopores inside fibers all contributed to the excellent solar reflectivity ($\approx$97%) and high emissivity ($>$0.96 between 8 and 13 μm) of a PVDF/tetraethyl orthosilicate (TEOS) membrane.[102] Moreover, hydrophobic SiO_2 nanoparticles were

selected to enhance the superhydrophobicity of a P(VdF-HFP) film obtained by electrospraying method.[103] Researchers often use Al_2O_3 and SiO_2 as fillers of polymer radiatve cooling matrix at the same time, which can improve the high reflectivity and show dual selectivity and broadband optical properties in IR region.[104] What's more, the composite radiative cooling membranes with gradient moisture absorption ability are more comfortable to wear.[105,106] In the study of Zhang et al.,[107] Al_2O_3 and SiO_2 served as fillers in the electrospinning and dip-coating processes to prepare a hierarchical metafabric (cellulose acetate (CA)/Al_2O_3 and polyamide 6 (PA6)/SiO_2) (Fig. 8d and e). It combined radiative cooling and wick-evaporation cooling to display high reflectivity of 99.16% in the visible band, and a high emissivity (78.13%) in the atmospheric transparency window. Covering a skin simulator with the meta-fabric reduced overheating by 16.6 °C, including the contribution of evaporative heat dissipation ($\sim$8.2 °C) caused by the gradient moisture absorption and evaporation. Alternatively, hollow SiO_2 microspheres have also been proposed as a multi-functional additive for composite coatings to enhance emissivity, replacing air voids or solid microspheres in the porous membranes for scattering, and resulting in lightweight coatings with good thermal insulation properties. Further, a mixture of broken glass bubbles and P(VdF-HFP) has been shown to increases the solar reflectivity from 93.3% (pristine glass bubbles) to 97.3%, with an emissivity of $\sim$93.4%[108] The tunability of the particle size and volume fraction of hollow spheres (or glass bubbles), which are already available as a commercial additive for high-end paint formulations, helps
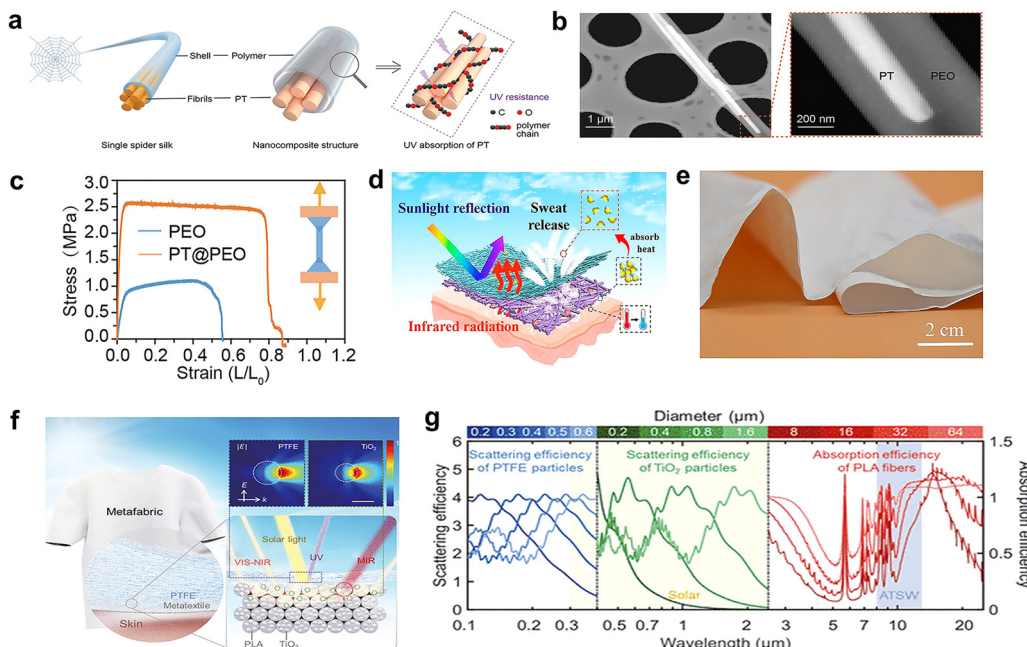
Fig. 8 (a) Schematic illustration of spider-silk-inspired $K_2Ti_6O_{13}$ doped PEO nanocomposite (PT@ PEO) structure. (b) TEM images with the PT@ PEO partial enlarged view. (c) Stress−strain curves of the PEO and PT@PEO film. Reproduced with permission from ref. 98. Copyright 2022, Wiley-VCH GmbH. (d) Schematic illustration of structure and optical properties and e, the photograph of the hierarchical metafabric. Reproduced with permission from ref. 107. Copyright 2022, American Chemical Society. (f) Schematic illustration of a metafabric structure and its passive daytime radiative cooling principle. Insets: The simulated scattering fields of 300 nm and 550 nm light by a 500 nm PTFE particle and a 400 nm TiO_2 particle. Scale bar:400 nm. (g) Calculation of scattering and absorption efficiencies of particles with different sizes in metafabric. PTFE particles, TiO_2 particles and PLA fibers. Reproduced with permission from ref. 110. Copyright 2021, American Association for the Advancement of Science.

achieving a high scattering efficiency, while the simple blending preparation process makes it appealing for practical applications. Furthermore, recent studies have mentioned that inorganic phosphate salts (PO_4^{3-}) has a high infrared emissivity required for radiative cooling, and as a filler of polymer matrix, it can increase the mechanical strength and tenacity of the structure.[109] A single-structured film is not conducive to the regulation of its spectral response over a wide spectrum. Multi-layer films can be therefore stacked to combine their different optical modulation capabilities. Zeng et al.[110] developed an optical metafabric with a hierarchical-morphology structure (TiO_2-polylactic acid (PLA) composite woven textile laminated by a polytetrafluoroethylene (PTFE) layer) that can be fabricated in large quantities (Fig. 8f), with excellent daytime radiative cooling capacity. Playing with the spatial structure, fiber structure, and internal microstructure of the fabric, the scattering efficiency in different spectral bands can be optimized with minimal crosstalk to realize the desired response in the 0.3–2.5 μm range (Fig. 8g). Thus, the solar reflection of the hierarchical-morphology metafabric can be optimized to 92.4%, combined with 94.5% emissivity in 8–13 μm, delivering day and night radiative cooling below ambient temperature.

5.2 Color inorganic filler composite polymer

Most of the proposed radiative cooling materials are white, in order to maximize the cooling performance. While for aesthetic reasons, this will limit their practical application.[111,112] Color materials or dyeing of white radiative cooling film will not affect the emissivity of them,[113] but will cause the material to absorb sunlight in the range of 300–700 nm, thus generating heat that weakens the cooling performance.[114,115] It will be a difficult task to generate daytime radiative cooling only depending on the radiative of the material. Therefore, PDMS with high emissivity is often used as the carrier of color materials, and the highly reflective Ag layer[47,116–118] and Al foil[119] are mostly used to neutralize the heat generated by color materials, which increases the preparation cost significantly. What's more, the silver layer is easy to be oxidized, which leads to the reduction of visible light absorption and corresponding cooling performance.

Similarly, multi-layer film composed of reflective layer and color layer in structure can improve the reflectivity of color film. Porous P(VdF-HFP) film with high reflectivity as the bottom layer can fully scatter the sunlight transmitted by the top layer (containing colorants), and achieve higher cooling performance and significantly lower temperature by virtue of its far higher infrared near-to-short wavelength reflectivity than commercial single layer coatings.[120] The introduction of fluorescent materials into the coating can convert the absorbed sunlight into fluorescent emission, thereby improving the effective solar reflectivity and cooling performance. In the research of Ma et al.,[121] the pigment ($SrAl_2O_4:Eu^{2+}$, Dy^{3+}, Yb^{3+}) can further reduce the sunlight absorption of commercial TiO_2 coatings using the fluorescence emission enhanced by Purcell effect (the reflectivity increased from 89.8% to 93.4%) to avoid the pursuit of extreme sunlight reflection (Fig. 9a). In subsequent studies,

by comparing the cooling capacity of coatings doped with $BaMgAl_{10}O_{17}:Eu^{2+}$ and $(Sr,Ba)SiO_4:Eu^{2+}$ respectively, they proved that the phosphor with smaller Stokes shift is the first choice to enhance reflectivity.[122] In addition, dyes with large band gaps (>4.13 eV) can be used for narrowband visible absorption.[123] However, this material needs to be excited under direct sunlight, and sometimes the color produced is not easy to be captured by the naked eye. Quantum dots (QDs) can absorb specific wavelength of visible to produce colors, and at the same time, the absorbed energy is reused to emit light of specific wavelengths through the photoluminescence effect, so the cooling capacity of color radiative cooling materials will not be significantly reduced in daytime. Yoon *et al.*,[124] deposited Cu-based QDs on the white film (hollow silica NPs and polymer blend films) sequentially to prepare colored radiative cooling films (yellow, red and brown) (Fig. 9b and c). The outdoor measurement results confirm that the yellow and red films can achieve a temperature drop of 3.25 °C and 0.51 °C respectively. The combination of electrostatic-spinning and ink-jet printing can be used to prepare patterned multi-colored radiative cooler (Fig. 9d). Among them, the top layer contains photoluminescent perovskite QDs that absorb and emit visible light of the desired color. The cellulose acetate (CA) nanofiber film (bottom layer) maximally backscatters the sunlight transmitted by the top layer, and radiates heat by the high mid-infrared emission (Fig. 9e). The temperature of green, yellow and red cooling films has reached 5.4–2.2 °C below ambient under sunlight.[125]

6. Development of organic based dynamic thermal management materials

Most radiative cooling systems are static, that is, the solar reflectivity and thermal emissivity are fixed after the material is fabricated. In hot weather, radiative cooling materials meet the cooling requirements, but in the case of low sunlight, an ideal material for thermoregulation should be able to limit heat losses or even harvest thermal energy from the sun to achieve thermal insulation or even heating. The sunlight can heat the interior of the highly-transmittaning solar materials, the highly-absorbing solar materials can achieve photothermal conversion,[88] and low infrared emitting materials can reduce long-wave radiation[126] all of which are suitable strategies for storing thermal energy. An additional dynamic mechanism was demonstrated by Zhang *et al.*,[127] who showed that a tunable infrared gating effect can be achieved by dynamically
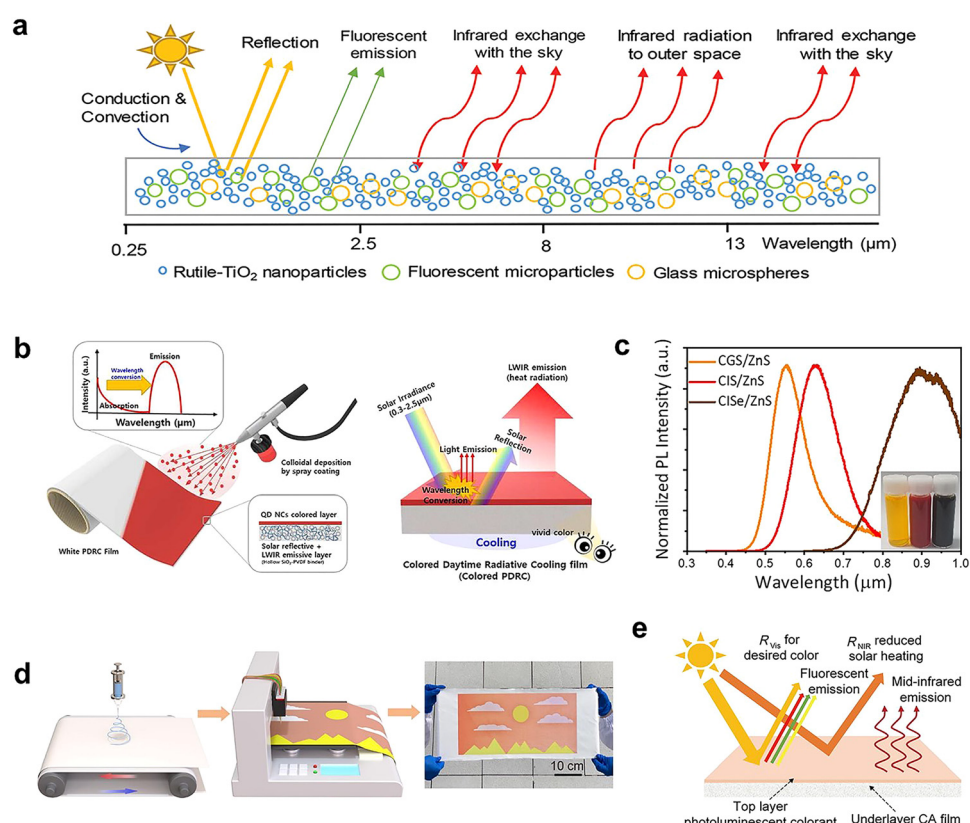
Fig. 9 (a) Schematics illustration of the fluorescent pigment coating and its optical mechanism. Reproduced with permission from ref. 121. Copyright 2020, Wiley-VCH GmbH. (b) Schematic illustration of the manufacturing and mechanism of the colored radiative cooling films. (c) Photoluminescence intensity of CGS/ZnS, CIS/ZnS, and CISe/ZnS quantum dot solutions. Reproduced with permission from ref. 124. Copyright 2021, Elsevier. (d) Schematic illustration of electrostatic- spinning and ink-jet printing process for multi-colored radiative cooler (photograph). (e) Schematic illustration of the bilayer photoluminescent perovskite QDs and CA nanofibers film with different optical functions. Reproduced with permission from ref. 125. Copyright 2022, Elsevier.

adjusting the distance between fibers in a textile, which in turn modulates their electromagnetic coupling.

This section is an extension of the functions of polymer based radiative cooling materials. The thermal management materials based on radiative cooling will have a broader scene in practical applications. We will discuss the different strategies to achieve composite dynamic temperature control materials that realize the function of temperature management based on radiative cooling. Table 2 summarize some crucial indicators of the organic-based dynamic thermal management materials in recent years.

6.1 Dual-mode materials

Janus membranes prepared by superimposing solar absorbing material and solar reflective material can realize the manually switching behavior between cooling and heating according to the environmental conditions. The laminated Janus membrane is optically stratified, but its multiple layers are mechanically bond together.[128] Metal nanoparticles,[129] metal nanowires,[88,130] and carbon materials[131] are often used as sunlight absorbing layers in the Janus membranes. The Janus films reported here need to be manually flipped to achieve cooling–heating switching, which is difficult for large area building materials. Li et al.[132] proposed the strategy of switching between cooling and heating by an electrostatically-controlled dual-mode device (Fig. 10a). The spectral characteristics of the cooling part (97.3% reflectivity, 94.1% emissivity) and the heating part (93.4% absorption, 14.2% emissivity) are completely opposite (Fig. 10b). This switching mode in the same plane can achieve building level thermal management through the reconfigurable interwoven arrangement of cooling–heating modules and dynamically switching overlapping sequence.[133] This way can be understood as the parallel placement of janus dual functional layers, if the motor is used to achieve rotation, it will still consume energy. As for the in situ cooling-photothermal switching strategy proposed Zhao et al.[134] A porous silicone membrane (Fig. 10c and d) can dynamically transition between porous state (93% solar reflection, 94% infrared emission) and solid-state (sunlight-transmitting) upon mechanical stimulation (Fig. 10e). The covered carbon black particles (CBPs) layer will be exposed and absorbed about 95% sunlight and raise the ambient temperature from 10 to 28 °C in the solid-state, showing the potential to provide all-round heat management under different ambient temperatures. Recently, a temperature driven zero-energy dual-mode thermal management device can realize the spontaneously switch between heating and cooling, intelligently (Fig. 10f and g).[135] The UV-Vis-IR absorptivity/emissivity spectrum of the device in heating (an aluminum plate coated with nano-chromium oxide powders) and cooling (dioctyl phthalate (DOP)-mod-ified poly(4-methyl-1-pentene) (PMP) encapsulating rutile titanium dioxide nanoparticles) modes is close to the ideal spectrum (Fig. 10h). This completely energy-free regulation mode is still the superposition of functional layers, which makes the preparation process more complicated. Thus, a kind of material that can control its own solar transmittance under external stimulation came into being.

6.2 Phase change materials

An important application of phase change materials is thermal management, which has been demonstrated with materials such as paraffin wax,[136–138] ester acids,[139] poly(ethylene glycol) (PEG)[140] and inorganic materials represented by VO_2.[15,141–143] A temperature control functionality for composites can be realized by combining the absorption and the heat storage-release ability of phase change materials with fiber fabrics with high porosity and low thermal conductivity. In a cold environment, phase change materials will solidify and release heat at the same time, providing a warmer environment. Conversely, with higher temperatures, the solid material will melt and absorb heat in the process, which will cooperate with the radiative cooling channel to further reduce the perceived temperature. Wu and coworkers used PEG to infiltrate thermally insulating fibers and enable personal thermal regulation (Fig. 11a).[144] After being coated by PDMS, the textile exhibited good bidirectional thermal insulation performance in the range between −20 °C and +90 °C, all combined with the strengthened mechanical stability and resistance of a textile. The low thermal conductivity and moisture absorption–evaporation ability of gel materials provide a more concise preparation strategy for the design of thermoregulating materials.[145] Their water evaporation capacity assists the radiative cooling to further increase the cooling potential, while the heat released by the hydrogel regeneration during the night can neutralize the temperature drop caused by radiative cooling. Thermochromic gels can also switch their appearance from transparent to white with

Table 2 Summary of information on various types of polymer

Material	Cooling mode			Heating mode			
	Reflectivity (%)	Emissivity (%)	$\Delta T_{\text{amb-cooler}}$	Optical modulation	Emissivity (%)	$\Delta T_{\text{amb-cooler}}$	Ref.
PVDF nanofiber/ZnO nanosheet/carbon nanotube/ Ag nanowire/PDMS	90.6	89.2	10.9 °C	Absorptivity 74.1%	10.5	−12.5 °C	130
PDMS, Cu/Zn, Ag, Cu, and PI dual-mode heating/ cooling material	97.3	94.1	—	Absorptivity 93.4%	14.2	—	132
Porous silicone film/coat it on carbon black particles	93	94	5 °C	Transmissivity 95%	94	−18 °C	134
Nano-Cr black Al plate/DOP-modified PMP matrix and TiO_2 NPs fillers	85	97	≈ 6 K	Absorptivity 91%	8	15 K	135
PVDF@PNIPAm film	82	96	1.8–3.7 °C	Reflectivity 12%	96	4.3–5.8 °C	150
Hierarchical porous coating	96.6	> 96	4.5 °C	Transmissivity 86.6%	> 96	$\Delta T_{\text{wet–dry}}$ = 47 °C	155
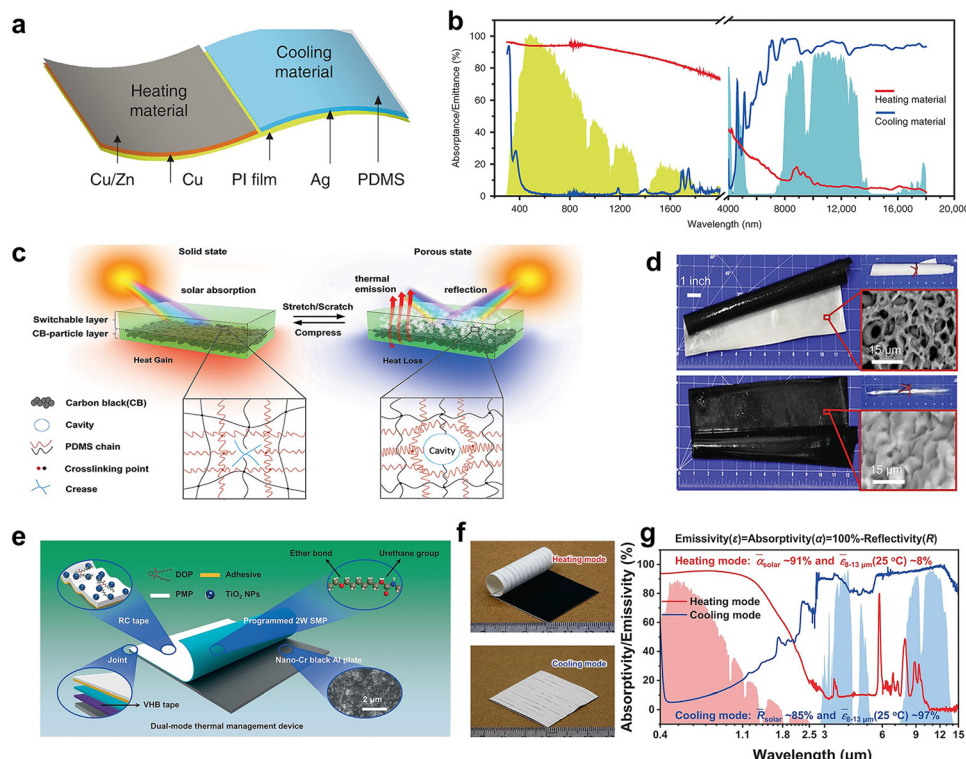
Fig. 10 (a) Structure diagram of dual-mode heating/cooling device. b, Spectral UV-Vis-IR absorptance/emittance of the dual-mode device. Reproduced with permission from ref. 132. Copyright 2020, Nature Publishing Group. (c) Schematic illustration of the double-layer structure composed of a switchable silicon. (d) The optical photo and the SEM images of a free-standing SPDMS2.0–CBP film in porous (top) and solid (bottom) states, respectively. Insets: The SPDMS2.0 single-layer film in different states. Reproduced with permission from ref. 134. Copyright 2020, Wiley-VCH GmbH. (e) Structural diagram, f, optical photo, g, Spectral UV-Vis-IR absorptivity/emissivity of the dual-mode device. Reproduced with permission from ref. 135. Copyright 2022, Nature Publishing Group.

changing temperature, thereby dynamically adjusting their transmittance.[146] Among them, a poly(N-isopropylacrylmide) (PNIPAm) hydrogel with high visible light transmission modulation and low critical solution temperature (~ 31 °C) has been reported.[147–149] The temperature responsiveness of this hydrogel is mainly realized by the water gradient discharge produced by the formation and breaking of hydrogen bonds between its structure and water molecules. The transparent or white state of the material corresponds to the difference between the ambient temperature and its phase transition temperature. The sandwich structure membrane composed of PNIPAm hydrogel and PVDF (Fig. 11b) exhibited up to 70% visible light reflection modulation (ΔR_{vis} = 70%) (Fig. 11c), radiative cooling efficiency of 1.8–3.7 °C during a hot day, and above-ambient solar heating of 4.3–5.8 °C in cold weather.[150] Overheating problems often occur in electronic devices, which will reduce the working efficiency or even burn the circuit itself. Similarly, with the advent of electric vehicles, the temperature of batteries should be controlled, and the air conditioning needs inside the vehicle can severely limit their driving range. Cover shields with good heat dissipation or cooling properties can improve the safety and lifetime of electric devices and batteries. With respect to applications in the building sector, however, additional requirements of reduced thickness and lightweight become relevant for these applications.

Phase-change material proposed by can respond Yang et al.[151] showed great potential in electronic thermal management applications, showing temperature reduction of electronic devices up to 5.5 °C due to its energy storage and passive radiative cooling features. Some smart phase change materials can work as the intelligent temperature detectors for biosafe wearable sensors and smart windows.[152] However, the optical properties of the phase change materials can not be adjusted according to personal thermal comfort needs, but can be adjusted according to the change of external temperature passively.

6.3 Solvent switching materials

For porous structured radiative cooling coatings, the switch between the transmittance and the reflectance modes can be realized through the wetting and drying (vapor-to-liquid transition) of the liquid (such as ethylene glycol, ethanol, acetic acid, glycerol, carbon tetrachloride, and cedar oilisopropanol (IPA) *etc.*) that matches its refractive index, so as to achieve the *in situ* thermal management.[153] In the dry mode (reflection), the strong Mie scattering of nanoscale pores ensures high solar reflectivity, while in the wet mode (transmission), the reduced interface scattering due to matched refractive index leads to high transmissivity. The P(VdF-HFP), PVDF, poly (methylmethacrylate), ethyl cellulose, and polystyrene can be used to
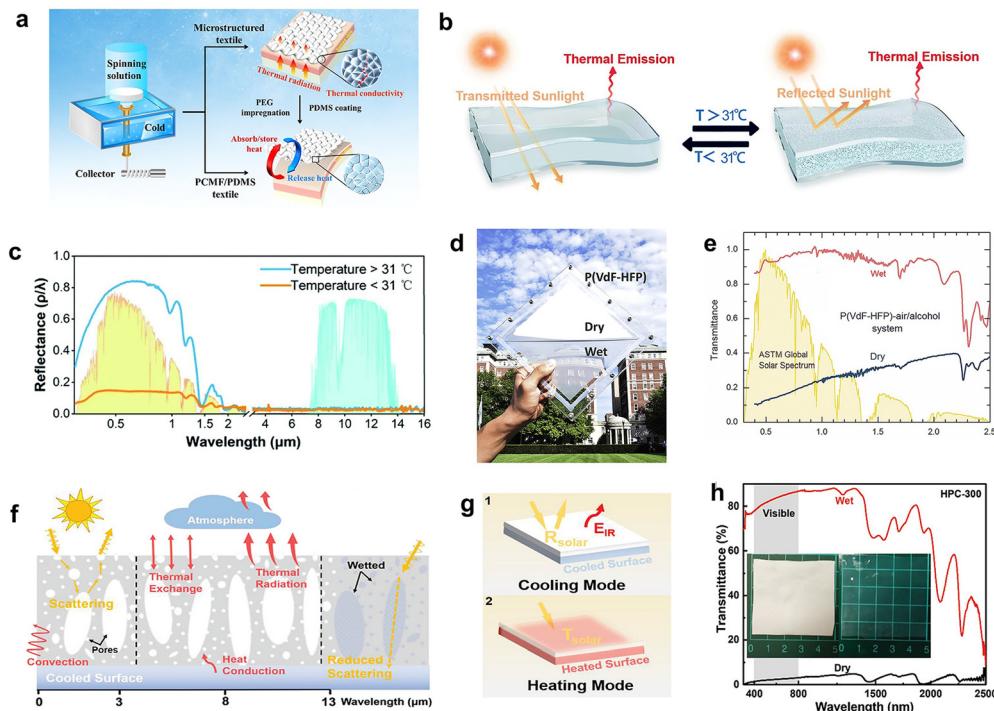
Fig. 11 (a) Schematic illustration of thermal insulation and temperature regulation textile manufacturing process. Reproduced with permission from ref. 114. Copyright 2020, American Chemical Society. (b) Schematic illustration and (c) Reflectance and emissivity spectra of the PVDF@PNIPAm film. Reproduced with permission from ref. 150. Copyright 2022, Royal Society of Chemistry. (d) Photograph and (e) spectral UV-Vis-IR transmissivity of the P(VdF-HFP) system in dry and wet states. Reproduced with permission from ref. 154. Copyright 2019, Cell Press. (f) Schematic diagram of the optical characteristic designed hierarchical porous structure. (g) The cooling and heating mode and (h) the spectral UV-Vis-NIR transmittance of the hierarchical porous coating in wet and dry state. Reproduced with permission from ref. 155. Copyright 2022, Wiley-VCH GmbH.

prepare polymer matrix in the researchs of reflection-transmission of solvent switched films (Fig. 11d and e).[154] The dual-mode heat regulation with switchable heating and cooling on a single hierarchical porous coating (HPC) was realized by Fei et al.[155] (Fig. 11f and g). It exhibited rapid switching between high solar reflectance ($\approx 96.6\%$) and high solar transmittance ($\approx 86.6\%$) in dry and wet states, respectively (Fig. 11h). Upon wetting, the refractive index contrast of the highly scattering and porous structure is significantly reduced, leading to a higher optical transmissivity which broadens its applicability, especially in regions with large seasonal temperature variation. This method is particularly suitable for thermal conditioning on various building surfaces requiring high solar reflectivity and high transmittance in the same film. However, it should be noted that the use of solvents is not very friendly to the environment, and will cause resource consumption.

7. Summary and outlook

This article provided an overview of the latest research results and developments in the field of organic-based radiative cooling materials, discussing their general properties and structure (alone or in combination with other materials), the main fabrication methods, and the range of heat management strategies that they enable. Based on the review and results discussed in this paper, organic-based membranes emerge as a prominent class of radiative cooling materials due to their wide availability,

simple and scalable fabrication, flexible application to different surfaces and textiles, as well as their recyclability potential. On the other hand, the UV radiation resistance of most organic materials is generally weaker than that of inorganic materials,[155] which raises concerns regarding their outdoor durability over long periods (>1 year). Improving the UV reflectivity can significantly enhance the reflectivity of the membrane in the solar spectrum and prolong the service life of polymer materials. Especially for applications in the building sector, fire-retardant and self-extinguishing properties are also desirable features that should be improved upon for organic materials, including their spectral stability under harsh environment conditions.[156] Although radiative cooling shows great potential in dry and temperate regions, few recent works suggest that polymer materials offer performance advantages in the cooling performance in tropical climates (high solar irradiance and high humidity).[64,157] Finally, due to the limitation of high reflectivity, most polymer radiative cooling materials are still white. From an aesthetic view, under the premise of ensuring reflection, color coolers are also a hot issue in future research.[83,112,115,125] Presently, the practical application of radiative cooling materials and polymer films is still not widespread, which highlights the need for a more quantitative analysis of their energy saving potential, as well as the costs associated to their fabrication, installation, maintenance and disposal throughout their life cycle.

In conclusion, organic-based materials hold great promise for the development of new cooling membranes and coatings.

Notably, the radiative cooling capacities of many single polymers is found to be comparable to that of composite materials, suggesting that any additional manufacturing steps required for the fabrication of the latter should be carefully evaluated in terms of the performance advantage it can bring. Coatings consisting of a single material are also preferable in terms of reduced costs and easier recycling, suggesting that this class of materials holds the most interesting engineering and commercial value for future research.

Author contributions

Xin Li: Conceptualization, data curation, and writing – original draft. Zhenmin Ding and Xueying Fan: Writing – review & editing. Lorenzo Pattelli, Linghao Kong and Hongbo Xu: Methodology, Validation, writing – review & editing. Lei Pan, Yao Li, and Jiupeng Zhao, Diederik S. Wiersma: Supervision.

Conflicts of interest

There are no conflicts to declare.

Acknowledgements

References

1 R. S. Ahima, *J. Clin. Invest.*, 2020, **130**, 559–561.

2 K. R. Miner, J. D'Andrilli, R. Mackelprang, A. Edwards, M. J. Malaska, M. P. Waldrop and C. E. Miller, *Nat. Clim. Change*, 2021, **11**, 809–819.

3 J. Zheng and S. Suh, *Nat. Clim. Change*, 2019, **9**, 374–378.

4 J. F. Nicol and S. Roaf, *Build. Res. Inf.*, 2017, **45**, 711–716.

5 J. Kim, Y. Zhou, S. Schiavon, P. Raftery and G. Brager, *Build. Environ.*, 2018, **129**, 96–106.

6 P. Hofmann, A. Walch, S. Arnold-Keifer, S. K. Selvarayan and G. T. Gresser, *Composites, Part A*, 2019, **126**, 105603.

7 R. Liu, X. Wang, J. Yu, Y. Wang, J. Zhu and Z. Hu, *Macromol. Mater. Eng.*, 2018, **303**, 1700456.

8 M. O. McLinden, C. J. Seeton and A. Pearson, *Science*, 2020, **370**, 791–796.

9 Y. Peng, L. Fan, W. Jin, Y. Ye, Z. Huang, S. Zhai, X. Luo, Y. Ma, J. Tang, J. Zhou, L. C. Greenburg, A. Majumdar, S. Fan and Y. Cui, *Nat. Sustainability*, 2022, **5**, 339–347.

10 M. He, Y. Sun and B. Han, *Angew. Chem., Int. Ed.*, 2022, **61**, e202112835.

11 D. Zhao, A. Aili, Y. Zhai, J. Lu, D. Kidd, G. Tan, X. Yin and R. Yang, *Joule*, 2019, **3**, 111–123.

12 Y. Yang, D. Rana, C. Q. Lan and T. Matsuura, *ACS Appl. Mater. Interfaces*, 2016, **8**, 15778–15787.

13 Y. Meng, J. Pu and Q. Pei, *Joule*, 2021, **5**, 780–793.

14 Y. Meng, Z. Zhang, H. Wu, R. Wu, J. Wu, H. Wang and Q. Pei, *Nat. Energy*, 2020, **5**, 996–1002.

15 K. Tang, K. Dong, J. Li, M. P. Gordon, F. G. Reichertz, H. Kim, Y. Rho, Q. Wang, C.-Y. Lin, C. P. Grigoropoulos, A. Javey, J. J. Urban, J. Yao, R. Levinson and J. Wu, *Science*, 2021, **374**, 1504–1509.

16 S. Fan and W. Li, *Nat. Photonics*, 2022, **16**, 182–190.

17 J. Jaramillo-Fernandez, H. Yang, L. Schertel, G. L. Whitworth, P. D. Garcia, S. Vignolini and C. M. Sotomayor-Torres, *Adv. Sci.*, 2022, **9**, 2104758.

18 E. Rephaeli, A. Raman and S. Fan, *Nano Lett.*, 2013, **13**, 1457–1461.

19 Z. Chen, L. Zhu, A. Raman and S. Fan, *Nat. Commun.*, 2016, **7**, 13729.

20 N. N. Shi, C.-C. Tsai, F. Camino, G. D. Bernard, N. Yu and R. Wehner, *Science*, 2015, **349**, 298–301.

21 T. Li, Y. Zhai, S. He, W. Gan, Z. Wei, M. Heidarinejad, D. Dalgo, R. Mi, X. Zhao, J. Song, J. Dai, C. Chen, A. Aili, A. Vellore, A. Martini, R. Yang, J. Srebric, X. Yin and L. Hu, *Science*, 2019, **364**, 760–763.

22 B. Orel, M. K. Gunde and A. Krainer, *Sol. Energy*, 1993, **50**, 477–482.

23 P. Berdahl, *Appl. Opt.*, 1984, **23**, 370–372.

24 H. Yuan, C. Yang, X. Zheng, W. Mu, Z. Wang, W. Yuan, Y. Zhang, C. Chen, X. Liu and W. Shen, *Opt. Express*, 2018, **26**, 27885–27893.

25 D. Chae, M. Kim, P.-H. Jung, S. Son, J. Seo, Y. Liu, B. J. Lee and H. Lee, *ACS Appl. Mater. Interfaces*, 2020, **12**, 8073–8081.

26 M. M. Hossain, B. Jia and M. Gu, *Adv. Opt. Mater.*, 2015, **3**, 1047–1051.

27 Y. Zhai, Y. Ma, S. N. David, D. Zhao, R. Lou, G. Tan, R. Yang and X. Yin, *Science*, 2017, **355**, 1062–1066.

28 J.-l Kou, Z. Jurado, Z. Chen, S. Fan and A. J. Minnich, *ACS Photonics*, 2017, **4**, 626–630.

29 L. Zhu, A. P. Raman and S. Fan, *Proc. Natl. Acad. Sci. U. S. A.*, 2015, **112**, 12282–12287.

30 C. Zou, G. Ren, M. M. Hossain, S. Nirantar, W. Withayachumnankul, T. Ahmed, M. Bhaskaran, S. Sriram, M. Gu and C. Fumeaux, *Adv. Opt. Mater.*, 2017, **5**, 1700460.

31 J. Mandal, Y. Yang, N. Yu and A. P. Raman, *Joule*, 2020, **4**, 1350–1356.

32 W. Jing, S. Zhang, W. Zhang, Z. Chen, C. Zhang, D. Wu, Y. Gao and H. Zhu, *ACS Appl. Mater. Interfaces*, 2021, **13**, 29558–29566.

33 B.-Y. Liu, C.-H. Xue, H.-M. Zhong, X.-J. Guo, H.-D. Wang, H.-G. Li, M.-M. Du, M.-C. Huang, R.-X. Wei, L.-G. Song, B. Chang and Z. Wang, *J. Mater. Chem. A*, 2021, **9**, 24276–24282.

34 J. Mandal, Y. Fu, A. C. Overvig, M. Jia, K. Sun, N. N. Shi, H. Zhou, X. Xiao, N. Yu and Y. Yang, *Science*, 2018, **362**, 315–319.

35 K. Zhou, W. Li, B. B. Patel, R. Tao, Y. Chang, S. Fan, Y. Diao and L. Cai, *Nano Lett.*, 2021, **21**, 1493–1499.

36 R. Xiao, C. Hou, W. Yang, Y. Su, Y. Li, Q. Zhang, P. Gao and H. Wang, *ACS Appl. Mater. Interfaces*, 2019, **11**, 44673–44681.

37 W.-Z. Song, X.-X. Wang, H.-J. Qiu, N. Wang, M. Yu, Z. Fan, S. Ramakrishna, H. Hu and Y.-Z. Long, *Nano Energy*, 2021, **82**, 105695.

38 X. Liu, C. Xiao, P. Wang, M. Yan, H. Wang, P. Xie, G. Liu, H. Zhou, D. Zhang and T. Fan, *Adv. Opt. Mater.*, 2021, **9**, 2101151.

39 G. Perrakis, A. C. Tasolamprou, G. Kenanakis, E. N. Economou, S. Tzortzakis and M. Kafesaki, *ACS Photonics*, 2022, **9**, 1327–1337.

40 D. Chae, S. Son, H. Lim, P. H. Jung, J. Ha and H. Lee, *Mater. Today Phys.*, 2021, **18**, 100389.

41 A. Leroy, B. Bhatia, C. C. Kelsall, A. Castillejo-Cuberos, M. Di Capua H., L. Zhao, L. Zhang, A. M. Guzman and E. N. Wang, *Sci. Adv.*, 2019, **5**, eaat9480.

42 C. Cai, Z. Wei, C. Ding, B. Sun, W. Chen, C. Gerhard, E. Nimerovsky, Y. Fu and K. Zhang, *Nano Lett.*, 2022, **22**, 4106–4114.

43 A. Aili, Z. Y. Wei, Y. Z. Chen, D. L. Zhao, R. G. Yang and X. B. Yin, *Mater. Today Phys.*, 2019, **10**, 100127.

44 B. Zhao, C. Guo, C. A. C. Garcia, P. Narang and S. Fan, *Nano Lett.*, 2020, **20**, 1923–1927.

45 Z. Yang and J. Zhang, *ACS Appl. Mater. Interfaces*, 2021, **13**, 43387–43395.

46 M. I. Iqbal, K. Lin, F. Sun, S. Chen, A. Pan, H. H. Lee, C.-W. Kan, C. S. K. Lin and C. Y. Tso, *ACS Appl. Mater. Interfaces*, 2022, **14**, 23577–23587.

47 Z. Ding, L. Pattelli, H. Xu, W. Sun, X. Li, L. Pan, J. Zhao, C. Wang, X. Zhang, Y. Song, J. Qiu, Y. Li and R. Yang, *Small*, 2022, **18**, 2202400.

48 B. Zhao, M. Hu, X. Ao, N. Chen, Q. Xuan, D. Jiao and G. Pei, *Appl. Energy*, 2019, **252**, 113432.

49 W. Wang, N. Fernandez, S. Katipamula and K. Alvine, *Renewable Energy*, 2018, **118**, 265–277.

50 H. Ma, L. Wang, S. Dou, H. Zhao, M. Huang, Z. Xu, X. Zhang, X. Xu, A. Zhang, H. Yue, G. Ali, C. Zhang, W. Zhou, Y. Li, Y. Zhan and C. Huang, *ACS Appl. Mater. Interfaces*, 2021, **13**, 19282–19290.

51 B. Zhu, W. Li, Q. Zhang, D. Li, X. Liu, Y. Wang, N. Xu, Z. Wu, J. Li, X. Li, P. B. Catrysse, W. Xu, S. Fan and J. Zhu, *Nat. Nanotechnol.*, 2021, **16**, 1342–1348.

52 D. Li, X. Liu, W. Li, Z. Lin, B. Zhu, Z. Li, J. Li, B. Li, S. Fan, J. Xie and J. Zhu, *Nat. Nanotechnol.*, 2021, **16**, 153–158.

53 I. Shepa, E. Múdra and J. Dusza, *Mater. Today Chem.*, 2021, **21**, 100543.

54 D. Zhong, J. Zhou and Y. Wang, *J. Membr. Sci.*, 2021, **632**, 119374.

55 M. Föllmer, S. Jestin, W. Neri, V. S. Vo, A. Derré, C. Mercader and P. Poulin, *Adv. Sustainable Syst.*, 2019, **3**, 1900082.

56 G. Kim, K. Park, K.-J. Hwang and S. Jin, *ACS Nano*, 2021, **15**, 15962–15971.

57 Y. N. Song, M. Q. Lei, J. Lei and Z. M. Li, *Mater. Today Energy*, 2020, **18**, 100504.

58 W. Zou, L. Pattelli, J. Guo, S. Yang, M. Yang, N. Zhao, J. Xu and D. S. Wiersma, *Adv. Funct. Mater.*, 2019, **29**, 1808885.

59 J. Syurik, G. Jacucci, O. D. Onelli, H. Hölscher and S. Vignolini, *Adv. Funct. Mater.*, 2018, **28**, 1706901.

60 J. Zhu, Z. An, A. Zhang, Y. Du, X. Zhou, Y. Geng and G. Chen, *iScience*, 2022, **25**, 104126.

61 J. Wang, J. Sun, T. Guo, H. Zhang, M. Xie, J. Yang, X. Jiang, Z. Chu, D. Liu and S. Bai, *Adv. Mater. Technol.*, 2022, **7**, 2100528.

62 C. Park, C. Park, X. Nie, J. Lee, Y. S. Kim and Y. Yoo, *ACS Sustainable Chem. Eng.*, 2022, **10**, 7091–7099.

63 X. Liu, M. Zhang, Y. Hou, Y. Pan, C. Liu and C. Shen, *Adv. Funct. Mater.*, 2022, **32**, 2207414.

64 T. Wang, Y. Wu, L. Shi, X. Hu, M. Chen and L. Wu, *Nat. Commun.*, 2021, **12**, 365.

65 L. Zhou, J. Zhao, H. Huang, F. Nan, G. Zhou and Q. Ou, *ACS Photonics*, 2021, **8**, 3301–3307.

66 J. Ni, Y. Zhang, Z. Song, P. Zhang, Y. Cao, Y. Yang, W. Wang and J. Wang, *Composites, Part A*, 2023, **164**, 107311.

67 L. Zhou, J. Rada, H. Zhang, H. Song, S. Mirniaharikandi, B. S. Ooi and Q. Gan, *Adv. Sci.*, 2021, **8**, 2102502.

68 W. Gao, Z. Lei, K. Wu and Y. Chen, *Adv. Funct. Mater.*, 2021, **31**, 2100535.

69 J. Li, Y. Liang, W. Li, N. Xu, B. Zhu, Z. Wu, X. Wang, S. Fan, M. Wang and J. Zhu, *Sci. Adv.*, 2022, **8**, eabj9756.

70 S. Son, Y. Liu, D. Chae and H. Lee, *ACS Appl. Mater. Interfaces*, 2020, **12**, 57832–57839.

71 W. Zou, H. Luo, M. Yang, J. Xu and N. Zhao, *Macromol. Rapid Commun.*, 2002, 2200695.

72 M.-C. Huang, C.-H. Xue, J. Huang, B.-Y. Liu, X.-J. Guo, Z.-X. Bai, R.-X. Wei, H.-D. Wang, M.-M. Du, S.-T. Jia, Z. Chen and Y. Lai, *Chem. Eng. J.*, 2022, **442**, 136239.

73 H. Zhong, Y. Li, P. Zhang, S. Gao, B. Liu, Y. Wang, T. Meng, Y. Zhou, H. Hou, C. Xue, Y. Zhao and Z. Wang, *ACS Nano*, 2021, **15**, 10076–10083.

74 H. Liu, J. Yu, S. Zhang and B. Ding, *Nano Lett.*, 2022, **22**, 9485–9492.

75 J. Liu, H. Tang, J. Zhang, D. Zhang, S. Jiao and Z. Zhou, *Energy Built Environ.*, 2023, **4**, 131–139.

76 M. Yang, W. Zou, J. Guo, Z. Qian, H. Luo, S. Yang, N. Zhao, L. Pattelli, J. Xu and D. S. Wiersma, *ACS Appl. Mater. Interfaces*, 2020, **12**, 25286–25293.

77 M. Alberghini, S.-d Hong, L. M. Lozano, V. F. Korolovych, Y. Huang, F. Signorato, S. H. Zandavi, C. P. Fucetola, I. Uluturk, M. Y. Tolstorukov, G. Chen, P. Asinari, R. Osgood, M. Fasano and S. V. Boriskina, *Nat. Sustainability*, 2021, **4**, 715–724.

78 Q. Tian, X. Tu, L. Yang, H. Liu, Y. Zhou, Y. Xing, Z. Chen, S. Fan, J. Evans and S. He, *Small*, 2022, 2205091.

79 C. Feng, P. Yang, H. Liu, M. Mao, Y. Liu, T. Xue, J. Fu, T. Cheng, X. Hu, H. J. Fan and K. Liu, *Nano Energy*, 2021, **85**, 105971.

80 J. Zhang, Z. Zhou, H. Tang, J. Xing, J. Quan, J. Liu, J. Yu and M. Hu, *ACS Appl. Mater. Interfaces*, 2021, **13**, 14132–14140.

81 Y. Tian, H. Shao, X. Liu, F. Chen, Y. Li, C. Tang and Y. Zheng, *ACS Appl. Mater. Interfaces*, 2021, **13**, 22521–22530.

82 Y.-N. Song, Y. Li, D.-X. Yan, J. Lei and Z.-M. Li, *Composites, Part A*, 2020, **130**, 105738.

83 W. Zhu, B. Droguet, Q. Shen, Y. Zhang, T. G. Parton, X. Shan, R. M. Parker, M. F. L. De Volder, T. Deng, S. Vignolini and T. Li, *Adv. Sci.*, 2022, **9**, 2202061.

84 S. Dong, Q. Wu, W. Zhang, G. Xia, L. Yang and J. Cui, *ACS Appl. Mater. Interfaces*, 2022, **14**, 4571–4578.

85 Z. Cheng, H. Han, F. Wang, Y. Yan, X. Shi, H. Liang, X. Zhang and Y. Shuai, *Nano Energy*, 2021, **89**, 106377.

86 J. López-Medina, W. O. F. Carvalho, J. Vazquez-Arce, E. Moncada-Villa, O. N. Oliveira Jr, M. H. Farías, H. Tiznado and J. R. Mejía-Salazar, *Nanotechnol.*, 2020, **31**, 505715.

87 J. Huang, D. Fan and Q. Li, *Mater. Today Energy*, 2022, **25**, 100955.

88 X. Yue, T. Zhang, D. Yang, F. Qiu, G. Wei and Y. Lv, *J. Mater. Chem. A*, 2019, **7**, 8344–8352.

89 J. Song, W. Zhang, Z. Sun, M. Pan, F. Tian, X. Li, M. Ye and X. Deng, *Nat. Commun.*, 2022, **13**, 4805.

90 B. Xiang, R. Zhang, Y. Luo, S. Zhang, L. Xu, H. Min, S. Tang and X. Meng, *Nano Energy*, 2021, **81**, 105600.

91 L. Cai, A. Y. Song, P. Wu, P. C. Hsu, Y. Peng, J. Chen, C. Liu, P. B. Catrysse, Y. Liu, A. Yang, C. Zhou, C. Zhou, S. Fan and Y. Cui, *Nat. Commun.*, 2017, **8**, 496.

92 C.-H. Xue, R.-X. Wei, X.-J. Guo, B.-Y. Liu, M.-M. Du, M.-C. Huang, H.-G. Li and S.-T. Jia, *Compos. Sci. Technol.*, 2022, **220**, 109279.

93 J. Fei, D. Han, J. Ge, X. Wang, S. W. Koh, S. Gao, Z. Sun, M. P. Wan, B. F. Ng, L. Cai and H. Li, *Adv. Funct. Mater.*, 2022, **32**, 2203582.

94 R. Liu, Z. Zhou, X. Mo, P. Liu, B. Hu, J. Duan and J. Zhou, *ACS Appl. Mater. Interfaces*, 2022, **14**, 46972–46979.

95 P. Li, A. Wang, J. Fan, Q. Kang, P. Jiang, H. Bao and X. Huang, *Adv. Funct. Mater.*, 2022, **32**, 2109542.

96 Z. Yang, Z. Zhou, H. Sun, T. Chen and J. Zhang, *Compos. Sci. Technol.*, 2021, **207**, 108743.

97 K.-Y. Chan, X. Shen, J. Yang, K.-T. Lin, H. Venkatesan, E. Kim, H. Zhang, J.-H. Lee, J. Yu, J. Yang and J.-K. Kim, *Nat. Commun.*, 2022, **13**, 5553.

98 P. Yao, Z. Chen, T. Liu, X. Liao, Z. Yang, J. Li, Y. Jiang, N. Xu, W. Li, B. Zhu and J. Zhu, *Adv. Mater.*, 2022, 2208236.

99 Y. Liu, X. Bu, M. He, S. Liang and Y. Zhou, *Sol. Energy*, 2022, **247**, 564–573.

100 H.-D. Wang, C.-H. Xue, X.-J. Guo, B.-Y. Liu, Z.-Y. Ji, M.-C. Huang and S.-T. Jia, *Appl. Mater. Today*, 2021, **24**, 101100.

101 C. Lin, Y. Li, C. Chi, Y. S. Kwon, J. Huang, Z. Wu, J. Zheng, G. Liu, C. Y. Tso, C. Y. H. Chao and B. Huang, *Adv. Mater.*, 2022, **34**, 2109350.

102 X. Wang, X. Liu, Z. Li, H. Zhang, Z. Yang, H. Zhou and T. Fan, *Adv. Funct. Mater.*, 2020, **30**, 1907562.

103 L.-C. Hu, C.-H. Xue, B.-Y. Liu, X.-J. Guo, J.-H. Wang and F.-Q. Deng, *ACS Appl. Polym. Mater.*, 2022, **4**, 3343–3351.

104 S. Son, T. Y. Lee, D. Chae, H. Lim, J. Ha, Y. K. Kim and H. Lee, *Adv. Opt. Mater.*, 2022, 2201771.

105 D. Miao, N. Cheng, X. Wang, J. Yu and B. Ding, *Chem. Eng. J.*, 2022, **450**, 138012.

106 D. Miao, N. Cheng, X. Wang, J. Yu and B. Ding, *Nano Lett.*, 2022, **22**, 680–687.

107 X. Zhang, W. Yang, Z. Shao, Y. Li, Y. Su, Q. Zhang, C. Hou and H. Wang, *ACS Nano*, 2022, **16**, 2188–2197.

108 X. Yu, F. Yao, W. Huang, D. Xu and C. Chen, *Renewable Energy*, 2022, **194**, 129–136.

109 S. Feng, Y. Zhou, C. Liu, T. Zhang, X. Bu, Y. Huang and M. He, *Chem. Eng. J.*, 2023, **452**, 139377.

110 S. Zeng, S. Pian, M. Su, Z. Wang, M. Wu, X. Liu, M. Chen, Y. Xiang, J. Wu and M. Zhang, *Science*, 2021, **373**, 692–696.

111 W. Xi, Y. Liu, W. Zhao, R. Hu and X. Luo, *Int. J. Therm. Sci.*, 2021, **170**, 107172.

112 Z. Ding, X. Li, X. Fan, M. Xu, J. Zhao, Y. Li and H. Xu, *Carbon Capture Sci. Technol.*, 2022, **4**, 100066.

113 L. Cai, Y. Peng, J. Xu, C. Zhou, C. Zhou, P. Wu, D. Lin, S. Fan and Y. Cui, *Joule*, 2019, **3**, 1478–1486.

114 H. Zhai, D. Fan and Q. Li, *Sol. Energy Mater. Sol. Cells*, 2022, **245**, 111853.

115 T. Wang, Y. Zhang, M. Chen, M. Gu and L. Wu, *Cell Rep. Phys. Sci.*, 2022, **3**, 100782.

116 S. Son, S. Jeon, D. Chae, S. Y. Lee, Y. Liu, H. Lim, S. J. Oh and H. Lee, *Nano Energy*, 2021, **79**, 105461.

117 R. A. Yalçın, E. Blandre, K. Joulain and J. Drévillon, *ACS Photonics*, 2020, **7**, 1312–1322.

118 S. Jeon, S. Son, S. Y. Lee, D. Chae, J. H. Bae, H. Lee and S. J. Oh, *ACS Appl. Mater. Interfaces*, 2020, **12**, 54763–54772.

119 S. Yu, Q. Zhang, Y. Wang, Y. Lv and R. Ma, *Nano Lett.*, 2022, **22**, 4925–4932.

120 Y. Chen, J. Mandal, W. Li, A. Smith-Washington, C.-C. Tsai, W. Huang, S. Shrestha, N. Yu, R. P. S. Han, A. Cao and Y. Yang, *Sci. Adv.*, 2020, **6**, eaaz5413.

121 X. Xue, M. Qiu, Y. Li, Q. M. Zhang, S. Li, Z. Yang, C. Feng, W. Zhang, J.-G. Dai, D. Lei, W. Jin, L. Xu, T. Zhang, J. Qin, H. Wang and S. Fan, *Adv. Mater.*, 2020, **32**, 1906751.

122 X. Ma, Y. Fu, A. Portniagin, N. Yang, D. Liu, A. L. Rogach, J.-G. Dai and D. Lei, *J. Mater. Chem. A*, 2022, **10**, 19635–19640.

123 J. Xu, R. Wan, W. Xu, Z. Ma, X. Cheng, R. Yang and X. Yin, *Mater. Today Nano*, 2022, **19**, 100239.

124 T. Y. Yoon, S. Son, S. Min, D. Chae, H. Y. Woo, J.-Y. Chae, H. Lim, J. Shin, T. Paik and H. Lee, *Mater. Today Phys.*, 2021, **21**, 100510.

125 X. Wang, Q. Zhang, S. Wang, C. Jin, B. Zhu, Y. Su, X. Dong, J. Liang, Z. Lu, L. Zhou, W. Li, S. Zhu and J. Zhu, *Sci. Bull.*, 2022, **67**, 1874–1881.

126 A. Yang, L. Cai, R. Zhang, J. Wang, P.-C. Hsu, H. Wang, G. Zhou, J. Xu and Y. Cui, *Nano Lett.*, 2017, **17**, 3506–3510.

127 X. A. Zhang, S. Yu, B. Xu, M. Li, Z. Peng, Y. Wang, S. Deng, X. Wu, Z. Wu and M. Ouyang, *Science*, 2019, **363**, 619–623.

128 W. Wang, Q. Zou, N. Wang, B. Hong, W. Zhang and G. P. Wang, *ACS Appl. Mater. Interfaces*, 2021, **13**, 42813–42821.

129 H. Luo, Y. Zhu, Z. Xu, Y. Hong, P. Ghosh, S. Kaur, M. Wu, C. Yang, M. Qiu and Q. Li, *Nano Lett.*, 2021, **21**, 3879–3886.

130 Y.-N. Song, M.-Q. Lei, D.-L. Han, Y.-C. Huang, S.-P. Wang, J.-Y. Shi, Y. Li, L. Xu, J. Lei and Z.-M. Li, *ACS Appl. Mater. Interfaces*, 2021, **13**, 19301–19311.

131 B. Dai, X. Li, T. Xu and X. Zhang, *ACS Appl. Mater. Interfaces*, 2022, **14**, 18877–18883.

132 X. Li, B. Sun, C. Sui, A. Nandi, H. Fang, Y. Peng, G. Tan and P.-C. Hsu, *Nat. Commun.*, 2020, **11**, 6101.

133 Y. Ke, Y. Li, L. Wu, S. Wang, R. Yang, J. Yin, G. Tan and Y. Long, *ACS Energy Lett.*, 2022, **7**, 1758–1763.

134 H. Zhao, Q. Sun, J. Zhou, X. Deng and J. Cui, *Adv. Mater.*, 2020, **32**, 2000870.

135 Q. Zhang, Y. Lv, Y. Wang, S. Yu, C. Li, R. Ma and Y. Chen, *Nat. Commun.*, 2022, **13**, 4874.

136 C. Yu, D. Shen, W. He, Z. Hu, S. Zhang and W. Chu, *Renewable Energy*, 2021, **178**, 1057–1069.

137 Y.-j He, Y.-y Xiao, R.-q Wang, D.-x Sun, J.-h Yang, X.-d Qi and Y. Wang, *Composites, Part A*, 2022, **162**, 107139.

138 J. Wu, M. Wang, L. Dong, J. Shi, M. Ohyama, Y. Kohsaka, C. Zhu and H. Morikawa, *ACS Nano*, 2022, **16**, 12801–12812.

139 C. Guo, Y. Miao and L. Li, *J. Renewable Sustainable Energy*, 2018, **10**, 064102.

140 J. Zhou, Y. Liu, Z. Yang, X. Wang, Y. Li, F. Liu, Z. Jiang, X. Sun, X. Li, Y. Zhao, C. Wang, S.-H. Ho and H. Yang, *Adv. Sustainable Syst.*, 2022, **6**, 2200132.

141 Y. Ke, Y. Yin, Q. Zhang, Y. Tan, P. Hu, S. Wang, Y. Tang, Y. Zhou, X. Wen, S. Wu, T. J. White, J. Yin, J. Peng, Q. Xiong, D. Zhao and Y. Long, *Joule*, 2019, **3**, 858–871.

142 M. Ono, K. Chen, W. Li and S. Fan, *Opt. Express*, 2018, **26**, A777–A787.

143 S. Wang, T. Jiang, Y. Meng, R. Yang, G. Tan and Y. Long, *Science*, 2021, **374**, 1501–1504.

144 J. Wu, R. Hu, S. Zeng, W. Xi, S. Huang, J. Deng and G. Tao, *ACS Appl. Mater. Interfaces*, 2020, **12**, 19015–19022.

145 Y. Sun, Y. Ji, M. Javed, X. Li, Z. Fan, Y. Wang, Z. Cai and B. Xu, *Adv. Mater. Technol.*, 2022, **7**, 2100803.

146 Y. Zhou, S. Wang, J. Peng, Y. Tan, C. Li, F. Y. C. Boey and Y. Long, *Joule*, 2020, **4**, 2458–2474.

147 J. Tian, H. Peng, X. Du, H. Wang, X. Cheng and Z. Du, *J. Alloys Compd.*, 2021, **858**, 157725.

148 Z. Fang, L. Ding, L. Li, K. Shuai, B. Cao, Y. Zhong, Z. Meng and Z. Xia, *ACS Photonics*, 2021, **8**, 2781–2790.

149 C. Lin, J. Hur, C. Y. H. Chao, G. Liu, S. Yao, W. Li and B. Huang, *Sci. Adv.*, 2022, **8**, eabn7359.

150 X. Mei, T. Wang, M. Chen and L. Wu, *J. Mater. Chem. A*, 2022, **10**, 11092–11100.

151 L.-Y. Yang, C.-P. Feng, L. Bai, R.-Y. Bao, Z.-Y. Liu, M.-B. Yang and W. Yang, *Chem. Eng. J.*, 2021, **425**, 131466.

152 G. Xu, H. Xia, P. Chen, W. She, H. Zhang, J. Ma, Q. Ruan, W. Zhang and Z. Sun, *Adv. Funct. Mater.*, 2022, **32**, 2109597.

153 C. Zhang, J. Yang, Y. Li, J. Song, J. Guo, Y. Fang, X. Yang, Q. Yang, D. Wang and X. Deng, *Adv. Funct. Mater.*, 2022, 2208144.

154 J. Mandal, M. Jia, A. Overvig, Y. Fu, E. Che, N. Yu and Y. Yang, *Joule*, 2019, **3**, 3088–3099.

155 J. Fei, D. Han, J. Ge, X. Wang, S. W. Koh, S. Gao, Z. Sun, M. P. Wan, B. F. Ng and L. Cai, *Adv. Funct. Mater.*, 2022, 2203582.

156 Y. Tian, X. Liu, J. Li, A. Caratenuto, S. Zhou, Y. Deng, G. Xiao, M. L. Minus and Y. Zheng, *Appl. Mater. Today*, 2021, **24**, 101103.

157 D. Han, J. Fei, J. Mandal, Z. Liu, H. Li, A. P. Raman and B. F. Ng, *Sol. Energy Mater. Sol. Cells*, 2022, **240**, 111723.